TU Clausthal

Clausthal University of Technology

Bachelor's Thesis

Jialun Jiang

Implementation and Evaluation of Metrics for Crash Point Determination for Aircraft Trajectory Risk Optimization

Bachelor's Thesis at Department of Informatics

First Censor: Prof. Dr. Sven Hartmann
Second Censor: Dr. Umut Durak
Third Censor: Prof. Dr. rer. nat. Joachim Schachtner

Date of Delivery: 02. March 2020

Eidesstattliche Erklärung

Hiermit versichere ich, dass ich die vorliegende Bachelor's Thesis

Implementation and Evaluation of Metrics for Crash Point Determination for Aircraft Trajectory Risk Optimization

selbstständig verfasst und keine anderen als die angegebenen Quellen und Hilfsmittel benutzt habe und dass alle Stellen dieser Arbeit, die wörtlich oder sinngemäß aus anderen Quellen übernommen wurden, als solche kenntlich gemacht wurden und dass die Arbeit in gleicher oder ähnlicher Form noch keiner anderen Prüfungsstelle vorgelegt wurde.

Des Weiteren erkläre ich, dass ich mit der öffentlichen Bereitstellung meiner Bachelor's Thesis in der Instituts- und/oder Universitätsbibliothek einverstanden bin.

This following english translation is for information purposes only.
The original german text above is the legally binding version.

I hereby ensure that I am the sole drafter of the work and did not use any sources and aids other than those listed, and that all portions of this work literally or analogously taken from other sources were labelled as such, and that the work has not been submitted in the same or similar form to any other evaluating entity.

Furthermore, I declare that I am willing to have my thesis made publicly available in the institute and/or university library

Clausthal-Zellerfeld, den 02. March 2020 (Jialun Jiang)

Abstract

In aviation, safety has always been an essential requirement. After more than a century of development, manned aviation has a sound risk management system, and its safety has been dramatically improved. Nevertheless, unmanned aviation is still a relatively new area, with the rapid popularization of UAV technology, it is becoming more and more necessary to improve the risk management and risk control of UAVs, for which trajectory optimization is a very effective method. The trajectory is adjusted according to the potential risks in the area around the trajectory, thereby avoiding high-risk areas and making the total potential risk of the trajectory smaller. So a risk map with sufficient accuracy and adequate generating time is essential for this method.

The risk map used this thesis is a two-dimensional grid map, where each cell of the map represents a real geographical area. Each cell has a risk value, which is used to measure the fatal injury caused by a UAV impact in this area. The calculation of the risk value is based on several factors, such as the location of the UAV, the area of the UAV, the radius of the UAV, types of accident, wind, population density, impact speed, impact angle, and whether the area is a no-fly zone. This calculation also needs to be done through various models, such as four different accident models, the wind model, and the casualty model. The population density map and the shelter map are also necessary for the calculation. They provide information on population density and shelter on the ground.

Evaluating the generated risk map is an indispensable step. In the evaluation of the generated risk maps, the dependencies of the input parameters and the resulting quality and its performance are identified. The goal is to derive parameters that enable an acceptable quality in a reasonable time. This means that the resulting risk map has to provide enough information to determine critically or even slightly increased risk for ground areas, but also has to be computed in a fast manner so that an alternative trajectory can be analyzed in a fast manner. The risk value itself is evaluated to make sure the risk is in a reasonable range.

Zusammenfassung

In der Luftfahrt war die Sicherheit schon immer eine sehr wichtige Anforderung. Nach mehr als einem Jahrhundert der Entwicklung verfügt die bemannte Luftfahrt über ein solides Risikomanagementsystem, und ihre Sicherheit wurde dramatisch verbessert. Aber die unbemannte Luftfahrt ist noch ein relativ neuer Bereich, und mit der raschen Verbreitung der UAV-Technologie wird es immer notwendiger, das Risikomanagement und die Risikokontrolle von UAVs zu verbessern, wofür die Flugbahnoptimierung eine sehr effektive Methode ist. Die Flugbahn wird entsprechend den potentiellen Risiken im Bereich um die Flugbahn herum angepasst, wodurch risikoreiche Gebiete vermieden und das potentielle Gesamtrisiko der Flugbahn verringert wird. Daher ist eine Risikokarte mit ausreichender Genauigkeit, die in einer akzeptablen Zeit erstellt werden kann„ für diese Methode unerlässlich.

Die in dieser Arbeit verwendete Risikokarte ist eine zweidimensionale Rasterkarte, bei der jede Zelle der Karte ein reales geografisches Gebiet darstellt. Jede Zelle hat einen Risikowert, der zur Messung der tödlichen Verletzung durch einen UAV-Einschlag in diesem Gebiet verwendet wird. Die Berechnung des Risikowertes basiert auf mehreren Faktoren, wie z.B. dem Standort des UAVs, dem Gebiet des UAVs, dem Radius des UAVs, Unfallarten, Wind, Bevölkerungsdichte, Aufprallgeschwindigkeit, Aufprallwinkel und ob das Gebiet eine Flugverbotszone ist. Diese Berechnung muss durch verschiedene Modelle durchgeführt werden, wie z.B. vier verschiedene Unfallmodelle, Windmodel und Unfallvorhersagemodel. Karten zur Bevölkerungsdichte und für Schutzräume im weitesten Sinne sind ebenfalls wichtig, da sie Informationen über die Dichte der Bevölkerung und geschützte Bereiche auf dem Boden geben.

Eine Auswertung der erstellten Risikokarte ist ebenfalls notwendig. In der Auswertung sind die Abhängigkeiten der Eingangsparameter und die daraus resultierende Qualität und Leistung identifiziert. Ziel ist die Ableitung von Parametern, die eine akzeptable Qualität in einer angemessenen Zeit ermöglichen. Das bedeutet, dass die resultierende Risikokarte genügend Informationen liefern muss, um ein kritisches oder sogar leicht erhöhtes Risiko für Bodenbereiche zu bestimmen, aber auch schnell berechnet werden muss, damit auch eine alternative Flugbahn schnell analysiert werden kann. Der Risikowert selbst wird bewertet, um sicherzustellen, dass sich das Risiko in einem angeme-ssenen Bereich befindet.

Contents

List of Figures

List of Tables

1 Introduction

Safety has always been a top priority in the aviation industry and is continually improving. According to the description in [21], commercial aviation safety has been dramatically improved since the birth of the aviation industry for more than a century, and it can be said that aviation is now the safest form of commercial transportation. At the same time, the unmanned aircraft system (UAS) technology has also significantly developed in recent decades. According to [20], the use of UAVs by military organizations around the world has increased, also in the civilian field, UAVs have many practical uses. So it becomes increasingly necessary to improve the risk management of UAVs.

Trajectory optimization is an effective method to control risks. It has existed for hundreds of years. According to [26], it was used to solve the Brachystochrone problem as early as 1697. With the advent of computers, it has become more and more practical. At first, it was only used in the aerospace industry, typical applications such as those described in [2]. Now it can also be used in other industries, such as UAVs trajectory optimization. For example, in [22], a trajectory optimization method based on UAV state estimates and information gathered by the imaging sensors were mentioned. It becomes more and more popular because it brings higher security, lower cost. Trajectory optimization can help to reduce the potential risk for people and structure on the ground, by choosing trajectories, which avoid traveling over areas with a high potential of damage for humans and structures.

Meanwhile, it is necessary to complete the trajectory optimization at an appropriate time. Otherwise, risk avoidance cannot be done in time. When estimating the risk, it must be considered that the causes of UAV accidents are diverse, so it is essential to explore different accident models. This thesis focuses on exploring the performance of calculating risks for a grid map for different accident models. The goal is to identify parameters, which provide sufficient quality for the risk map but can be computed in an acceptable time.

The thesis has the following structure: in this chapter, the author first introduces the background of writing this thesis and the contributions of previous researchers in related fields, then briefly introduces the work done in this thesis and presents its overview in the form of a flowchart.

1.1 Previous Work

Although the risk assessment of UAVs is a relatively new field compared to manned aviation, there are still many experts and scholars, which have done much research in this field: These papers explain the relationship between unmanned aviation risk assessment and manned aviation risk assessment: According to [10], [25], the current

risk assessment of UAVs is mainly derived from the risk assessment of manned aviation. However, the risk assessment of unmanned aviation is not the same as that of manned aviation; As early as 2004, JAA (Joint Aviation Authorities) has already discussed the development of European UAV's regulations and proposed that the benchmark for UAVs should be the benchmark certified by manned aviation [15].

These papers provide some frameworks for the safety of UAV operations: The researcher in [19] developed a set of quantified risk criteria for UAS operations. This criterion meets the requirements of the As Low As Reasonably Practicable (ALARP) risk management framework used in current regulatory practice. [6] provided a framework for structuring operational safety cases for UAVs, the author tried to manage the risk of a Mid-Air Collision (MAC) accident to an acceptable level and developed the barrier bow-tie model to structure the safety case for generic UAS operations.

Different UAV risk assessment and risk management methods are proposed in these papers, and an author has found problems with existing methods and wants to improve them: The unique aspects of applying security risk management processes to UAS are described in [4]. The failure rate is vital for the risk assessment of UAS, a method to determine a failure rate requirement for UAV critical systems called the equivalent level of safety (ELOS) analysis are used in [17]. [5] proposed a new formula risk analysis tool in the absence of experience of UAS operational hazards and proposed a simple casualty model. [10] presents a method to quantify the probability of fatalities, which are caused by different descent events of UAV. [24] used a two-dimensional location-based map to quantify the risk when UAV flies over a specified area with given population density. Some problems of the existing models are mentioned in [30], such as not considering the impact distribution, or using overly complicated methods to calculate. Therefore, an effective calculation method is proposed for estimating the impact distribution of fixed-wing UAVs.

It is also necessary to pay attention to the most popular new technologies of UAVs, such as BVLOS(Beyond Visual Line of Sight), miniaturization: Today, the beyond visual line of sight operation is very common in UAVs. The ground-based detect and avoid (GBDAA) capability is mentioned in [12], which is required for the beyond visual line of sight operation of UAVs, so an infrastructure that can guide safety assured design of future UAS missions that use GBDAA is developed. Due to the unreliability of small UAV systems, and they are also prevalent types of UAVs, it is necessary to analyze their failure modes. Related work was completed in [13]. For further risk assessment of UAS is also helpful. The researcher in [14] also presented a comprehensive simulation and flight test facility for reliability and fault-tolerance of small UAS. A framework for reliability assessment of small scale Unmanned Aerial Vehicle was also developed in [27].

1.2 Current Work

This work aims to generate a UAV's risk map for trajectories and also in a fast dynamically manner to determine the time that a computer needs to generate the risk map and how to optimize the time cost and also the quality of the risk map. It contains the

area near the flight path of the UAV so that the flight path can be adjusted to make the flight less risky for people on the ground. The generating of the risk map was inspired by [24]. The accident models in [10] are used in this thesis to calculate the risk values of the risk map. Those models can predict the possible impact location of the aircraft after a specific type of accident, or it gives a two-dimensional probability density function. The probability of a particular area is obtained by integrating the function. Then the wind model adds wind effect to those accident models because the wind will change the position of the point of impact. A map containing possible impact points is generated by the accident models and the wind model, which is called the impact map in this thesis.

The next step is to generate a risk map. First, it is necessary to determine whether the flight area is inside the no-fly zone through the fly zone map. If so, instead of calculating the risk value, a negative value constant represents high risk will be set. This is to avoid spending additional resources to calculate and also to warn the aircraft to avoid the area. After that, the casualty can be predicted based on the information of impact points. Casualties are affected by factors such as population density, shelter, and parameters of the UAV itself, which is mentioned in [9], [11] and [20], so it is necessary to build the population density map and shelter map. When this part of the work is done, calculate the risk value of the risk map by using the casualty model. The whole process is demonstrated by the flowchart in Fig. 1.1:

The final part of this thesis is to implement a risk map using previous models and evaluate them. In the evaluation, the dependencies of the input parameters and the resulting quality and performance are contained. The goal is to derive parameters that enable an acceptable quality in a reasonable time. This means that the resulting risk map has to provide enough information to determine critically or even slightly increased risk for ground areas, but also has to be computed in a fast manner, so that also an alternative trajectory can be analyzed in a fast manner. The risk value itself is evaluated to make sure the risk is in a reasonable range.

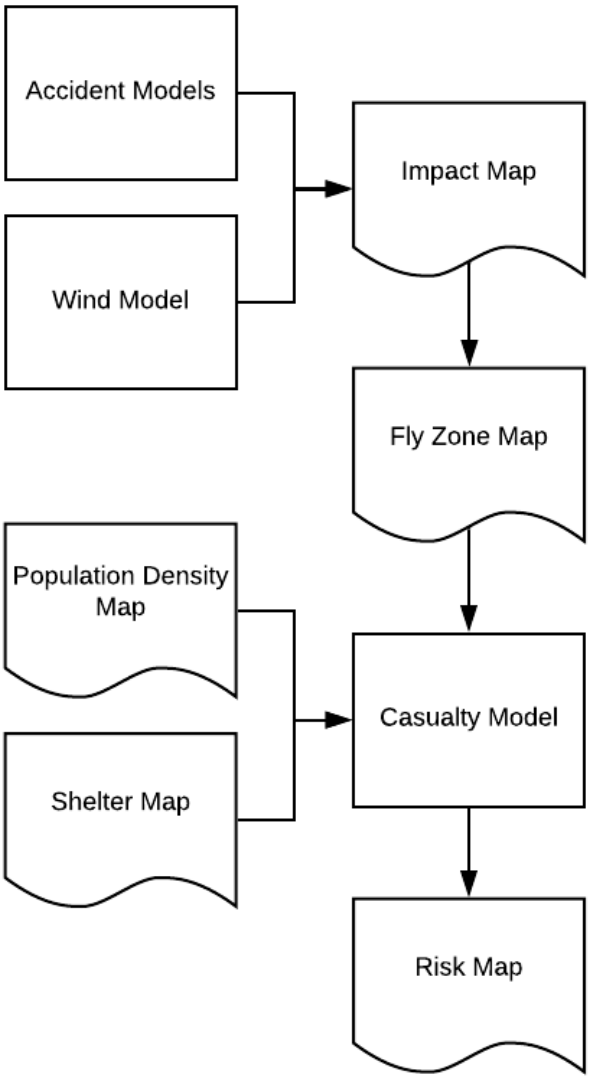

Figure 1.1: The process of generating a risk map

2 Methods

In this chapter, definitions and models will be described in detail. These are also the theoretical basis for the implementation: First, a detailed definition of the risk map used in this thesis is given. Afterward, some types of no-fly zones and four types of UAV accidents are introduced. The probability of a UAV accident is also necessary to calculate the risk value. Some UAV accident types also have different accident models, which can be used to predict the location or probability of the UAV hitting the ground. The impact of wind on the UAV's crash site is distinct and must be taken into account. Population density, as well as ground shelters, are also relevant. They will affect the estimate of casualties, which is the calculated risk value.

2.1 Risk Map

The risk map used this work is a two-dimensional grid map, where each cell of the map represents a real geographical area. Each cell has a risk value, which is used to measure the fatal injury caused by a UAV impact in this area. The calculation of the risk value is based on several factors, such as the location of the UAV, the area of the UAV, the radius of the UAV, types of accident, wind, population density, impact speed, impact angle, and whether the area is a no-fly zone. An overview for all input parameters can be seen in table 3.1. Each cell represents a real area of $n \times n\ m^2$. An appropriate value of n should be chosen. If it is too large, it cannot accurately represent the change of risk value. However, if it is too small, The cost of calculation is unbearable.

2.2 Fly Zone

The no-fly zone is airspace where aircraft are prohibited from flying. No-flying usually has the following reasons:

- **Air traffic control:** The relevant authorities coordinate and guide different flights in the airspace or airport to prevent aircraft from accidents, and to maintain high efficiency of air traffic. It is sometimes also based on particular needs, such as to control the airspace above essential meetings or events.

- **Airport:** Due to frequent flights taking off and landing over the airport, it is necessary to prohibit the flight of other air vehicles in the airspace. Otherwise, other aircraft could affect flight safety.

- **Natural preservation zone:** When the aircraft is flying over a natural preservation zone, if it crashes, it may cause damage to the ecosystem of the zone and even cause a fire. Such accidents must be avoided.

- **Military area:** In order to protect the safety of military aircraft and prevent military secrets from leaking, it is also common to establish a no-fly zone in military areas.

- **Densely populated area:** This is the area like square, business district, residential area. If the aircraft crashes in such places is likely to cause harm to people, so it is also necessary to set up a no-fly zone.

Due to the particularity of the no-fly zone, in this thesis, the risk value of the no-fly zone is set directly to a negative value. Because on the one hand, in reality, UAVs flying into such areas will bring some immeasurable risks, on the other hand, the main focus of this thesis is on calculating risk values, and the no-fly zones will be pruned for the given instances.

2.3 Types of Accidents

There are many types of accidents that cause UAV crashes. In this thesis, the accident models in [10] are mainly used. These models cover most types of UAV accidents and can be used to calculate possible impact points and speed at impact. The impact points and impact speed are useful for further calculating of the final risk value. There are four types of UAV accidents:

- **Ballistic descent:** If the UAV loses lift, such as a wing is broken or the motor is damaged, a ballistic descent will happen. The ballistic descent is determined only by the aerodynamics of the damaged aircraft.

- **Uncontrolled glide:** If the UAV loses its thrust, but the fuselage structure is intact, then it will glide uncontrollably.

- **Parachute descent:** Some UAVs are equipped with parachutes. If the aircraft system detects a serious error, it will open the parachute and descend.

- **Flyaway:** If the UAV loses control and enters autopilot mode, the aircraft will be controlled by the autopilot system, then it will fly to the maximum flight distance for the given fuel.

The respectively model for the accidents will be explained in detail in 2.5. Nevertheless, before that, this thesis will focus on the probability of accidents.

2.4 Probability of Accidents

The probability of UAV accidents is affected by many factors, and there are many types of accidents. In this thesis alone are four types of accidents mentioned. So it is not very easy to estimate this probability directly. In [11], the National Transportation Safety Board (NTSB) accident data from 1984 to 2004 was analyzed, and the UAS fatality rate was recommended to be set to 10^{-7} or less. The accident rate should be less than the fatality rate because the accident does not necessarily cause fatal injury to people. In [7], the concept of Failure Probability Objectives (FPOs) is used, which means the maximum acceptable likelihood of occurrence of a failure of a given level of severity. In a NASA(National Aeronautics and Space Administration) paper [1], the author used the Bayesian belief networks (BBNs) to model and estimate the probability of UAS accidents. In this model, causal factors and outcomes are linked to each other to form a network. The possibility of accidents of the UAV is calculated more accurately through real-time data from the UAV, such as the data of GPS Count, GPS Status, Remaining Battery, Battery Voltage, and Telemetry Health. However, since the real-time data of the UAV in this project are usually not easy to obtain, the probability of FPOs from Table 2.1 as the probability of accidents will be used in this thesis because it is already the maximum acceptable likelihood of occurrence of a failure, the UAV failure rate in reality generally does not greater than this value.

2.5 Models of Accidents

Four accident models, corresponding to the four different types of accidents mentioned in section 2.3 are used. The input values of the models are usually physical constants such as gravity acceleration, air density, and drag coefficient, as well as some basic parameters of the UAV, such as flying height, UAV weight, UAV speed, and glide ratio, and so on. These models return possible impact points, impact speeds, and especially for the flyaway model, which returns a two-dimensional probability density function for calculating the probability of impact on different locations.

2.5.1 Ballistic Descent

In the model, the UAV loses lift, such as a wing is broken or the motor is damaged, then the ballistic descent happens. It is determined only by the aerodynamics of the damaged aircraft. Since this model is too comprehensive, this thesis only lists the main formulas that will be used from the model. For more derivation details, please see [18]. First, the constants and parameters to be used next are listed in Table. 2.2

The overall integral conditions are:

$$\hat{H}_{\mathrm{d}} = \operatorname{arctanh}(\hat{v}_{\mathrm{y,i}}\gamma), \hat{H}_{\mathrm{u}} = \arctan(\hat{v}_{\mathrm{y,i}}\gamma), \hat{G}_{\mathrm{d}} = \ln\cosh(\hat{H}_{\mathrm{d}}), \hat{G}_{\mathrm{u}} = \ln\cosh(\hat{H}_{\mathrm{u}}) \tag{2.1}$$

where $\Gamma = \sqrt{mg/c}$ is the terminal velocity (gravitational force and drag force are equal with opposite signs) and $\gamma = \frac{1}{\Gamma}$, $\hat{v}_{\mathrm{y,i}} = max(0, v_{\mathrm{y,i}})$. The aircraft will first have a rising

Table 2.1: Catastrophic Failure Condition FPOs for Different Classes of UAS [7]

UAS Class	**FPO for All UAS Catastrophic Failure Conditions ($\mathbf{FPO_{SYS}}$)**	**FPO for Individual UAS Catastrophic Failure Conditions ($\mathbf{FPO_{IND}}$)**
UAS-25 Large Transport Aircraft	$APF_{\mathrm{SYS}} \leq 10^{-7}$	$APF_{\mathrm{IND}} \leq 10^{-9}$
UAS-23 Class I	$APF_{\mathrm{SYS}} \leq 10^{-5}$	$APF_{\mathrm{IND}} \leq 10^{-7}$
UAS-23 Class II	$APF_{\mathrm{SYS}} \leq 10^{-6}$	$APF_{\mathrm{IND}} \leq 10^{-8}$
UAS-23 Class III	$APF_{\mathrm{SYS}} \leq 10^{-7}$	$APF_{\mathrm{IND}} \leq 10^{-9}$
UAS-27 Small Rotorcraft	$APF_{\mathrm{SYS}} \leq 10^{-5}$	$APF_{\mathrm{IND}} \leq 10^{-7}$
UAS-29 Large Rotorcraft	$APF_{\mathrm{SYS}} \leq 10^{-6}$	$APF_{\mathrm{IND}} \leq 10^{-8}$
UAS-VLA Very Light Aircraft	$APF_{\mathrm{SYS}} \leq 10^{-5}$	$APF_{\mathrm{IND}} \leq 10^{-7}$
UAS-VLR Very Light Rotorcraft	$APF_{\mathrm{SYS}} \leq 10^{-5}$	$APF_{\mathrm{IND}} \leq 10^{-7}$
UAS below that of CPA weights operating beyond visual line of sight (UAS-BVLOS)	$APF_{\mathrm{SYS}} \leq 10^{-4}$	$APF_{\mathrm{IND}} \leq 10^{-6}$
UAS below that of CPA weights operating within visual line of sight (UAS-WVLOS)	$APF_{\mathrm{SYS}} \leq 10^{-4}$	$APF_{\mathrm{IND}} \leq 10^{-6}$

Table 2.2: Nomenclature for Ballistic Descent Model

Symbol	**Meaning**
m	Weight
g	Gravity acceleration
ρ	Air density
A	Frontal area
y	Flight altitude
C_{D}	Drag coefficient
$v_{\mathrm{x,i}}$	Initial speed in x direction
$v_{\mathrm{y,i}}$	Initial speed in y direction

process in the ballistic descent, and then begin to fall after rising to the highest point, and finally hit the ground. So the time when an aircraft is at its highest altitude needs to be calculated:

$$\hat{t}_{\text{top}} = -\frac{\Gamma}{g}\text{arctanh}(\gamma min(0, v_{\text{y,i}})) \tag{2.2}$$

and the horizontal distance traveled for reaching highest altitude:

$$x_{v_{\text{x}}}(t) = \frac{m}{c}\ln(1 + v_{\text{x,i}}ct/m), x_1 = x_{v_{\text{x}}}(\hat{t}_{\text{top}}), \hat{t}_{\text{c}} = t_c(\hat{t}_{\text{top}}, \hat{H}_{\text{d}}) \tag{2.3}$$

The time of crossing the point where $v_x = v_y$ should be:

$$t_c = \frac{m(gt_{top} - \Gamma H_{\text{d}} + v_{\text{x,i}}(1 + (H_{\text{d}} - g\gamma t_{\text{top}})^2)}{mg + cv_{\text{x,i}}(gt_{\text{top}} - \Gamma H_{\text{d}})} \tag{2.4}$$

The distance from flight altitude to highest altitude is:

$$y_{\text{top}} = -\frac{m}{2c}\ln(1 + (\gamma min(0, v_{\text{y,i}}))^2) \tag{2.5}$$

After the airplane has passed the highest altitude, it will begin to fall, the time taken for this process is:

$$t_{\text{drop}} = (\text{arccosh}(\exp(\frac{cy}{m} + G_{\text{d}})) - H_{\text{d}})\frac{\Gamma}{g}, \hat{t}_{\text{drop}} = t_{\text{drop}}(y - y_{\text{top}}, \hat{H}_{\text{d}}, \hat{G}_{\text{d}}) \tag{2.6}$$

The total time for the entire ballistic descent is:

$$\hat{t}_{\text{im}} = \hat{t}_{\text{top}} + \hat{t}_{\text{drop}} \tag{2.7}$$

the horizontal velocity at highest altitude is also needed:

$$v_{\text{x,top}} = \frac{mv_{\text{x,i}}}{m + v_{\text{x,i}}c\hat{t}_{\text{top}}} \tag{2.8}$$

so that the horizontal distance traveled from highest altitude to the point where $v_{\text{x}} = v_{\text{y}}$ can be calculated:

$$x_2 = \frac{m}{c}\ln(1 + cv_{\text{x,top}}\frac{min(\hat{t}_{\text{im}}, \hat{t}_{\text{c}}) - \hat{t}_{\text{top}}}{m}) \tag{2.9}$$

and the horizontal and vertical velocities at the time of crossing:

$$v_{\text{x,c}} = \frac{mv_{\text{x,i}}}{m + v_{\text{x,i}}c\hat{t}_{\text{c}}}, v_{\text{y,c}} = \Gamma\tanh(g\gamma(\hat{t}_{\text{c}} - \hat{t}_{\text{top}}) + \hat{H}_{\text{d}}) \tag{2.10}$$

The horizontal distance of the last part of the whole process is the distance traveled from the point where $v_{\text{x}} = v_{\text{y}}$ to the impact point, which is calculated as:

$$H_{\text{c}} = \text{arctanh}(\gamma v_{\text{y,c}}), G_{\text{c}} = \ln\cosh(H_{\text{c}}), t = \hat{t}_{\text{im}} - \hat{t}_{\text{c}}, \tag{2.11}$$

Table 2.3: Nomenclature for Uncontrolled Glide Model

Symbol	Meaning
γ	Glide ratio
y	Flight altitude
v_{g}	Horizontal glide speed

$$x_3 = \frac{v_{\mathrm{x,c}} e^{G_{\mathrm{c}}} \Gamma}{g} (\arctan(\sinh(g\gamma t + H_{\mathrm{c}})) - \arcsin(\gamma v_{\mathrm{y,c}})) \tag{2.12}$$

Finally, the total horizontal distance should be:

$$x = x_1 + x_2 + x_3 \tag{2.13}$$

With the total horizontal distance, the impact point of the UAV can be estimated, but in order to estimate the casualties caused by the aircraft, the impact speed is still needed, which is calculated as:

$$v_{\mathrm{x,im}} = \begin{cases} v_{\mathrm{x,c}} e^{G_{\mathrm{c}}} \operatorname{sech}(g\gamma(\hat{t}_{\mathrm{im}} - \hat{t}_{\mathrm{c}}) + H_{\mathrm{c}}) & \text{if } \hat{t}_{\mathrm{im}} > \hat{t}_{\mathrm{c}}; \\ \frac{m v_{\mathrm{x,i}}}{m + v_{\mathrm{x,i}} c \hat{t}_{\mathrm{im}}} & \text{if } \hat{t}_{\mathrm{im}} \leq \hat{t}_{\mathrm{c}}. \end{cases} \tag{2.14}$$

$$v_{\mathrm{y,im}} = \Gamma \tanh(\frac{g}{\Gamma}(\hat{t}_{\mathrm{im}} - \hat{t}_{\mathrm{c}}) + \hat{H}_{\mathrm{d}}) \tag{2.15}$$

Because the aircraft structure in this accident model is incomplete, the final crash point will be close to where the aircraft disintegrated in the air and follow the original flight direction of the aircraft.

2.5.2 Uncontrolled Glide

When the aircraft loses power, but the aircraft structure remains intact, the aircraft will glide along the original flight direction. The known quantities required for this model are in the table 2.3: Glide ratio represents the horizontally traveled distance per vertically descended distance, which is the most critical factor in the gliding process. Then the horizontal distance x traveled in an uncontrolled glide from altitude y can be calculated through the formula:

$$x(y) = \gamma y \tag{2.16}$$

Based on the horizontal distance $x(y)$ calculated above and the horizontal glide speed, the drop time can be calculated:

$$t_{\mathrm{drop}}(y) = \frac{x(y)}{v_{\mathrm{g}}} \tag{2.17}$$

In this model, the aircraft has a complete structure and glides, so the crash point of the aircraft will be far from the position where the aircraft lost control in the air and started to glide and in the direction of glide.

Table 2.4: Nomenclature for Parachute Descent Model

Symbol	Meaning
A_{p}	Parachute area
$C_{\mathrm{d,p}}$	Parachute drag coefficient
m	Parachute weight
g	Gravity acceleration

2.5.3 Parachute Descent

Similarly, for this model, some constants need to be known in advance. they will be found in the table 2.4. Parachute descent is a relatively simple process, the aircraft detects the fault in the aircraft system and open the parachute, then reduce the horizontal velocity to zero instantly, however, please note that in [10] it is mentioned that there is a delay between the detection of the fault in the aircraft system and the opening of the parachute. Since the distance traveled by aircraft during this time has little effect on the final impact point, it can be ignored. With additional physical constants and parameters of the parachute, the descending speed of the parachute can be calculated as:

$$v_{\mathrm{drop}} = \sqrt{\frac{2mg}{A_{\mathrm{p}} C_{\mathrm{d,p}}}} \tag{2.18}$$

So the drop time from flight altitude y should be:

$$t_{\mathrm{drop}} = \frac{y}{v_{\mathrm{drop}}} \tag{2.19}$$

In this model, because the aircraft will open the parachute and descend slowly, the final crash point will be closer to the location of the aircraft break down in the air than the uncontrolled glide but farther away than the ballistic descent. However, the influence of the initial flight direction on the crash point is no longer evident but is more affected by external factors, such as wind.

2.5.4 Fly-away

When the UAV loses control and enters autopilot mode, the aircraft will be controlled by the autopilot system, and then it will fly to the maximum flight distance for the given fuel. The flight direction can be in any direction, either hovering in the air or flying in one direction. Constants and parameters that this model needs to use are in Table 2.5. According to [10], the model consists of two contributions:

- In the first part, the possibility of a ground impact is considered to decrease linearly with distance from the event point and reach zero in the maximum range, the possibility of a ground impact is considered to decrease linearly with the distance from the event point and reach zero at the maximum range because in this case,

Table 2.5: Nomenclature for Fly-away Model

Symbol	Meaning
θ	Wind average direction
$R_{\max}$	Maximum flight range given the available fuel
v_c	Aircraft cruise airspeed
$p = (p_N, p_E)$	North-east position relative to the event point

the aircraft will cruise over the event point until the fuel is exhausted. However, considering this movement is random, the probability of hitting the ground at any point within the flight circumference is equal, that is, the probability should decrease with the square of the distance, as a compromise the author in [10] chooses a linear relationship and also take into account the effect of the wind. Finally, this is modeled as:

$$f(p) = max[0, \underbrace{R_{\max} - ||p||}_{\text{linear decrease}} + \underbrace{\cos(\arctan\frac{p_N}{p_E} + \theta)\frac{||p||}{v_c}}_{\text{modification according to wind}}] \tag{2.20}$$

- In the second part, since the aircraft ascends more or less in the vertical direction, which causes the ground impact point to be close to the event point, this part is modeled as a normal distribution based on the distance to the event point, with a mean of 0 and a standard deviation of σ_{va}:

$$g(p) = \frac{1}{2\pi\sigma_{va}^2}\exp\left(-\frac{||p||^2}{2\sigma_{va}^2}\right) \tag{2.21}$$

Finally, the two parts are linearly combined, and their weights are equal:

$$P_{\text{flyaway}}(p) = (1-\beta)\frac{f(p)}{\iint_{-\infty}^{\infty} f(p)} + \beta g(p), \beta = 0.5 \tag{2.22}$$

In this model, the aircraft is hovering in the air or always flying in one direction until the fuel is exhausted so that the crash point may be any direction centered on the aircraft's original position.

2.6 Model of Wind

The wind has a significant influence on all four types of events. Since the fly-away model has already considered the effects of wind, the wind model will only be used in the other three accident models, such as ballistic descent, uncontrolled glide, and parachute descent. Two main factors determine the wind: wind speed and direction. It can be modeled by using the normal distribution, or according to data from the authorities, the data can be real-time or historical.

Table 2.6: Nomenclature for Wind Model

Symbol	Meaning
y	Flight altitude
θ	Flight direction
ψ	Wind direction
w	Wind speed
x	Traveled distance from accident model
t	Drop time from accident model

According to the description of [10], since all other aerodynamic characteristics have been considered in these three models, the offset caused by the wind depends only on the drop time. Please note that the drop time has been determined in these three models, so the wind effect will only be in the horizontal direction, so only the wind in the horizontal direction needs to be considered. The detailed calculation formula for the offset caused by the wind can be found in [18], but first, the data in Table 2.6 is needed. The travel distance of the aircraft as it descends is used, then use this distance add the horizontal offset caused by the wind, finally get the possible impact points after being affected by the wind:

$$p(y) = \begin{bmatrix} \cos\theta & -\sin\theta \\ \sin\theta & \cos\theta \end{bmatrix} \begin{bmatrix} x(y) \\ 0 \end{bmatrix} + w \begin{bmatrix} \cos\psi \\ \sin\psi \end{bmatrix} t(y) \tag{2.23}$$

It should also be noted that the impact speed from the previous model also needs to be combined with the wind speed. Because after the wind acts on the aircraft, the aircraft will have a speed in the wind direction. This speed needs to be combined with the original flight speed of the aircraft to obtain the speed affected by the wind. The calculation process is as follows:

1. Calculate the angle between flight direction θ wind direction ψ: $|\psi - \theta|$
2. Calculate the resultant speed of flight speed, and wind speed v_1, here need to use the angle calculated in the previous step and the law of cosines:

$$v_1 = \sqrt{v_{\text{flight}}^2 + v_{\text{wind}}^2 + 2v_{\text{flight}}v_{\text{wind}}\cos(|\psi - \theta|)} \tag{2.24}$$

3. Calculate the resultant speed of drop speed and v_1 using the Pythagorean theorem, because v_1 is still in the horizontal plane and the direction of v_{drop} is vertically downward:

$$v_2 = \sqrt{v_1^2 + v_{\text{drop}}^2} \tag{2.25}$$

2.7 People Density

Population density is an essential factor in the risk assessment of UAV, if the UAV hit the ground, the change in population density will have a significant influence on the

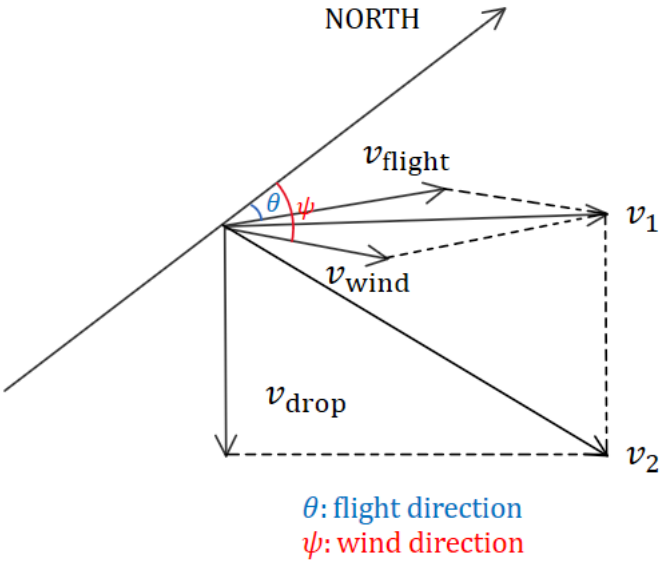

Figure 2.1: Final Speed Calculation

probability of the UAV hitting any person. If there is a flight accident in a densely populated area, it is straightforward to hit people, which is why, as mentioned in section 2.2, UAV flight is usually prohibited in densely populated areas.

Population density data can usually be obtained from government agencies, such as the bureau of statistics or the city hall. Another new method for estimating population density using mobile phone data is mentioned in [16], which has a unique advantage over traditional methods, it can obtain relatively real-time population density data, this is very important because the difference in population density is enormous for different periods in the same place. Please recall the risk map concept mentioned in section 2.1, which consists of a number of cells, each representing a real geographic area of size $n \times n$ m^2. Based on the population density data obtained, it will also be generated as a grid map. The size of each cell is the same as the risk map's cell and contains information about population density. For this thesis, historical data of population distributions in Germany is used to create instances.

2.8 Sheltering Effects

Another factor that influences the risk value is the shelter because the damage caused by the same impact event is very different for people hiding in office buildings and exposed to open spaces. In [1], the author divides the shelter into four categories according to their safety, see Table 2.7. In order to quantify their sheltering effect, from no shelter to D class, values from $[0, 10]$ are assigned to them, called sheltering parameter, where no

Table 2.7: Building Classes [1]

Roof Class	Description
A	Mobile homes and trailers Temporary office trailers
B	Single family dwellings Duplex and fourplex residential dwellings Small condominiums and townhouses Small apartment buildings
C	Small retail commercial buildings Small office and medical office buildings
D	Public buildings Warehouses Manufacturing plants

Table 2.8: Nomenclature for Casualty Estimation

Symbol	Meaning
m	UAV weight
γ	Impact angle
v_{imp}	Impact velocity
ρ	People density
W_{ua}	Wing span
L_{ua}	Length of the UAV
H_{p}	Height of a person
R_{p}	Radius of a person
p_{s}	Sheltering parameter

shelter is 0 and D class is 10.

However, please note that it is difficult to obtain such detailed building information in reality. So a compromise is provided in [24], which is to divide the shelter into two categories: for areas with building information set the sheltering parameter to 7.5, the area missing building information set the sheltering parameter to 2.5, these value will be used in section 2.9 to calculate the probability of fatality.

2.9 Casualty Estimation

First, the meaning of the required symbols is defined in Table 2.8. If the UAV hits the ground, it is necessary to estimate the size of the impact area. There is a frequently

used formula for this from [20]:

$$A_{\text{exp}} = (W_{\text{ua}} + 2R_{\text{p}})(L_{\text{ua}} + \frac{H_{\text{p}}}{\tan\gamma} + 2R_{\text{p}}) \tag{2.26}$$

Moreover, this thesis also gives a schematic diagram 2.2 for easy understanding. Ac-

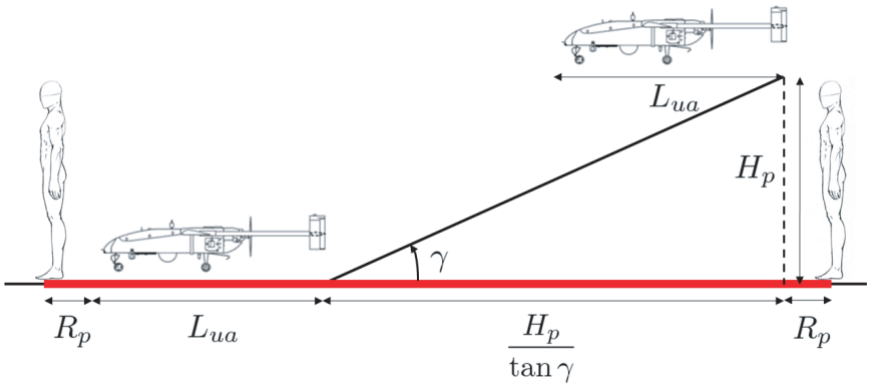

Figure 2.2: Impact Area Calculation [20]

cording to the description in the figure, the aircraft rushed to the ground at a γ angle, and it would glide a distance of the fuselage length L_{ua} after hitting the ground.

Then based on the population density obtained in Section 2.7, the number of people present in the crash area can be calculated and as a result exposed to the accident:

$$N_{\text{exp}} = A_{\text{exp}} \cdot \rho \tag{2.27}$$

In order to further calculate the casualties, the probability of fatal injury when a person is exposed to an accident can be calculated as $P(fatality|exposure)$.

According to the description in [11], kinetic energy plays a key role in calculating the probability of fatality, but there is no consensus in the literature on the relationship between kinetic energy and fatality. The results calculated by the models used in different papers are very different. Therefore, a logistic curve based on the kinetic energy impact is finally selected, which is mentioned in [9] and is considered to be a good model for estimating fatality:

$$P(\text{fatality}|\text{exposure}) = \frac{1}{1 + \sqrt{\frac{\alpha}{\beta}}[\frac{\beta}{E_{\text{imp}}}]^{\frac{1}{4p_{\text{s}}}}} \tag{2.28}$$

where E_{imp} is the kinetic energy at impact, can be calculated by the Work-Energy Theorem:

$$\frac{1}{2}m \cdot v_{\text{imp}}^2 \tag{2.29}$$

Furthermore, α is the impact energy required for a fatality probability of 50% with $p_{\text{s}} = 0.5$, β is the impact energy required to cause a fatality as ps goes to zero. Please

Table 2.9: Fatality rates from analysis of NTSB accident data between 1984 and 2004.

Accident type	**Accident rate**
Total	$5.60 \cdot 10^{-5}$
Resulting in fatality	$1.09 \cdot 10^{-5}$
Resulting in fatality on the ground	$1.48 \cdot 10^{-7}$

note that since the sheltering parameter range used here is $[0, 1]$, and the sheltering parameter range set in section 2.8 is $[0, 10]$, it needs to be normalized.

Finally, the expected number of fatalities N_{fatality} can be given by the following formula:

$$N_{\text{fatality}} = N_{\text{exp}} \cdot P(\text{fatality}|\text{exposure}) \tag{2.30}$$

This value will be used as the risk value. In order to determine whether this risk value is meaningful and reliable, it is necessary to continue to study it.

According to previous research, there are some papers that study the risk assessment of UAV and give some estimated casualty rates, such as [3], [23], [28], but these predicted values are different, ranging from 10^{-9} to 10^{-5}. Different institutions and scholars also have various requirements for the acceptable level of risk from UAS. First, a survey of US Navy in [8] showed that the Range Safety Criteria for UAS should have a fatality rate of less than 10^{-6}. Then the conclusions based on historical data of manned aviation are also worth considering. Because according to the description from [10] and [25], the current risk assessment of UAVs is mainly derived from the risk assessment of manned aviation. In [3], the NTBS accident data from 1984 to 2004 was analyzed, the results can be found in table 2.9. For UAV, it can be considered that its fatality rate is less than 10^{-7}, which is consistent with manned aviation. The author in [29] thinks that the limit should be smaller: 10^{-8}. In [5] a range from 10^{-9} to 10^{-6} is used for research. In summary, a range from 10^{-9} to 10^{-6} can be considered as a reasonable range of risk value.

So far, all necessary theoretical basis of the following chapters has been clearly described.

3 Case Study

This chapter is about the conception of the model, and then the actual data will be used for research.

3.1 Conception

First, accident models in section 2.5 need to be implemented, the input values required by the model are listed in the tables 2.2, 2.4, 2.3, 2.5. The specific formula can also be found in 2.5, for the model ballistic descent, uncontrolled glide, parachute descent, they will return the horizontal displacement distance and the final impact speed. It can get an impact position by parameters such as the flight direction of the input. For the probability of these flight accidents, the probability in 2.1 is be used. Then the wind effect is added, which is mentioned in section 2.6 and has a further influence on the impact location. For the model flyaway, it directly gives a two-dimensional probability density function that takes into account the wind effect. By double-integrating, the appropriate region, the probability of hitting an area after a flyaway accident is obtained. Next, the model in section 2.9 will be used to estimate the casualty. This model will use the final speed given by the accident model, and the given population density and the condition of the shelter. Finally, a risk map based on the estimated casualties is generated. It is also necessary to choose the appropriate size and resolution for the risk map. The size should not be too large, because if the resolution is also large, it will take too much time to get the results.

However, if the resolution is too small, it is difficult to see the change in risk value. Because the model ballistic descent, uncontrolled glide, parachute descent will output possible impact locations, the size of the risk map will be chosen by the following method: First, the possible impact points are calculated from the accident model, and then the size of the risk map is selected based on the points at the impact point and the flight path. The risk map should contain all the points. For the model flyaway, since it directly gives the probability value of a specific area being hit, the appropriate area to integrate should be selected, and this area can not be too large. Otherwise, it will be difficult to see the change of the risk value, and if it is too small, the cost of calculation is too high.

3.2 Implementation

The following sections will introduce the specific implementation methods of the models and risk maps used in this thesis.

3.2.1 Development Environment

In this thesis, `python` is used to implement models. Because its syntax is simple and also has a variety of powerful packages. First, pandas is used to process the flight data which usually contain the information about aircraft type, aircraft locations and flight altitude in the aircraft path, please note that because the aircraft location is usually represented by latitude and longitude coordinate system, it needs to be converted to a coordinate which uses distance. For each location, there is also the data of aircraft velocity, flight direction, and rate of climb. According to the given aircraft type, parameters of the aircraft can be found from the manufacturer, which are needed in the accident models. Python also has `numpy` and `scipy` for scientific calculation, they will be used to build the model.

3.2.2 Implementation of No-fly Zone

According to section 2.2, the implementation of no-fly zone is quite simple, if the no-fly zone needs to be considered, the risk value in the no-fly zone area is directly set to a negative value.

3.2.3 Implementation of Accident Models

The four accident models will be defined as four different functions. The input values for these functions are listed in tables 2.2, 2.4, 2.3, 2.5, then the formula mentioned in 2.5 will be implemented by using `numpy`, please note that for the model flyaway in 2.5.4, `integrate.dblquad` function from `scipy` will be needed for the calculation of double integrals. As mentioned in section 2.5, these models will return possible impact points, impact speeds, but please note that for the flyaway model, it will return a two-dimensional probability density function for calculating the probability of impact on different locations. Please recall the particularity of the flyaway model mentioned in section 2.5, and according to 3.1 the appropriate area to integrate needs to be selected. By integrating the two-dimensional probability density function of the flyaway model, it can be found that most of the impacts occurred in a circle with the accident point as the center and R_{max} mentioned in the table 2.5 as the radius, which means that only integrate within the range of the circle can get the probability of hitting different areas in this circle. Because the circle (ring) area is to be integrated, it is necessary to convert the probability density function of the flyaway with the Cartesian coordinate system into the probability density function with the polar coordinate system. The converted probability density function is as follows:

$$f(p) = max[0, R_{\max} - r + \frac{\cos(\alpha + \theta)r}{v_c}]r \tag{3.1}$$

$$g(p) = \frac{1}{2\pi\sigma_{\text{va}}^2} \exp\left(-\frac{r^2}{2\sigma_{\text{va}}^2}\right) r \tag{3.2}$$

Table 3.1: Parameter settings for further research

Symbol	Meaning	Value
m	Weight of UAV	3.75 kg
g	Gravity acceleration	9.82 m/s^2
ρ	Air density	1.3 kg/m^3
y	Flight altitude	515.87 m
$v_{\mathrm{x,i}}$	Initial speed in x direction	22.79 m/s
$v_{\mathrm{y,i}}$	Initial speed in y direction	4.86 m/s
C_{D}	Drag coefficient at ballistic descent	$N(0.7, 0.2)$
γ	Glide ratio	$N(12, 2)$
v_{g}	Horizontal glide speed	16 m/s
A_{p}	Parachute area	12.5 m^2
$C_{\mathrm{d,p}}$	Drag coefficient at parachute descent	$N(1.14, 0.2)$
R_{max}	Maximum flight range given the available fuel	1000 m
v_{c}	Aircraft cruise airspeed	21 m/s
θ	Flight direction	0.51
ψ	Wind direction	$N(1.24, 0.17)$
w	Wind speed	$N(7, 2)$ m/s

Finally, the two parts are still linearly combined and their weights are equal:

$$P_{\mathrm{flyaway}}(p) = (1-\beta)\frac{f(p)}{\iint_0^\infty f(p)} + \beta g(p), \beta = 0.5 \tag{3.3}$$

please note that the range of the double integral becomes 0 to ∞, which means that the radius of the integrated circle is from 0 to ∞.

Examples of different accident models are shown in figure 3.1. The possible impact points of the accident are shown through a heat map. Aircraft position is where ballistic descent happens, wind direction and flight direction are also shown in the figure. The parameter settings for examples are listed in the table 3.1.

3.2.4 Implementation of Wind Model

The formula of the wind model has been listed in section 2.6. It should be noted here that this model applies to three accident models other than the flyaway model because the flyaway model has already considered the influence of wind.

3.2.5 Implementation of Population Density Map

If there is relevant population density map data, the population density map grid can be directly mapped to the risk map grid one by one to get the corresponding population

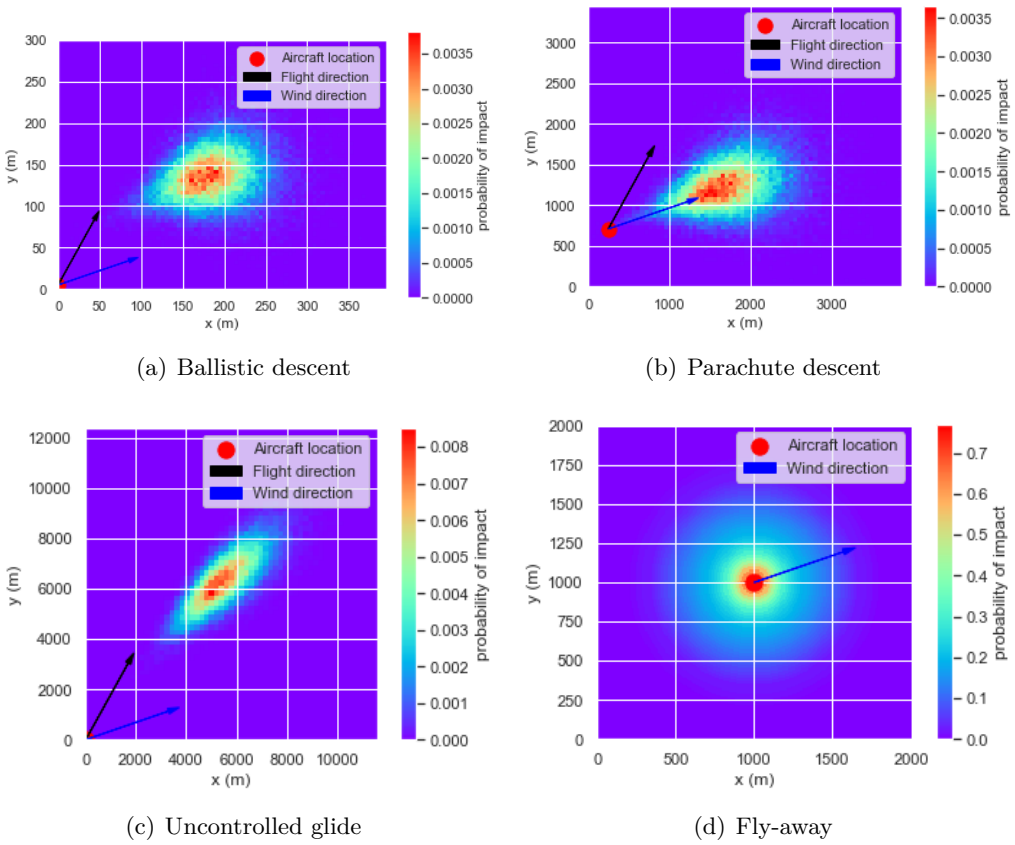

(a) Ballistic descent

(b) Parachute descent

(c) Uncontrolled glide

(d) Fly-away

Figure 3.1: Example of accident models

density value. Since no relevant data was obtained at the time of writing this thesis, for convenience, the Gaussian mixture is directly used to generate the population density map. First, create a map of the same size as the impact map, and store the map information through a two-dimensional array, for each cell on the map, set a random initial value within a certain range as the initial population density value. Then randomly select some cells on the map as the center of the densely populated area. The position of the center is created by the uniform distribution. The covariance matrix is also needed; it determines the size of the densely populated area, which is how dispersed the population is in this area. Finally, the multivariate uniform distribution is used to generate some cells near the center and set a higher population density values than initial population density values to represent the densely populated area. An example of a people density map is shown in Figure 3.2(a).

Alternatively, more simply, use the average population density value of the area where the experiment is located. Since this article was written in Germany, the related experiments in the future will also be mainly in Germany. Therefore, the average population density value of Germany is used: 232 persons per square kilometer.

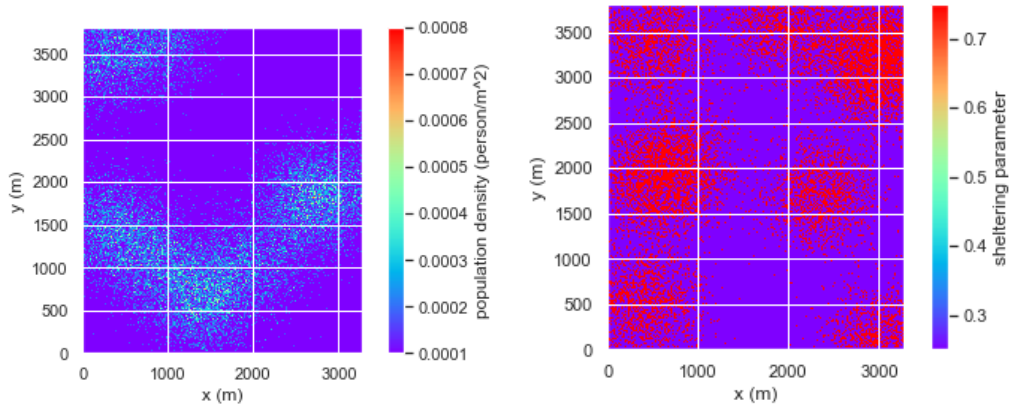

(a) Population density map

(b) Sheltering map

Figure 3.2: Example of population density map and sheltering map

3.2.6 Implementation of Sheltering Map

Compared to population density information, building roof class data is more difficult to obtain. Four different building roof classes are mentioned in Table 2.7, but in reality, there is usually no specific data set to distinguish these building roof classes. Therefore a similar method to the population density map is used to create the sheltering map. Now the center represents the center of building dense area. For the cells near the center, the sheltering parameter is set to 7.5, which means the area with shelter, for any other cells, is 2.5, which means the area without shelter. An example of a people density map is shown in Figure 3.2(b).

3.2.7 Implementation of Casualty Estimation Model

The implementation details of this model have been discussed in 2.9. Parameter settings can also be found in Table 3.1. Some parameters have not been set, such as the impact angle. The calculation method can be found in section 2.9 and Figure 2.1, but please note that for the fly-away model, the impact angle is directly set to $\pi/4$ because the data required to calculate the impact angle is not included in the model. The population density value p, and the sheltering parameter p_s can also be obtained from the population density map and the sheltering map. In addition the parameter α (Impact energy required for a fatality of probability of 50% with $p_s = 0.5$) is set to $10^6 j$, and β (Impact energy required to cause a fatality as ps goes to zero) to $10^2 j$.

3.2.8 Generation of Risk Map

The risk value is visualized by the risk map. A good risk map can clearly show the change in the risk value in different areas. The quality of the risk map is mainly affected by the following three parameters:

- **Number of samples:** Ballistic Descent, Uncontrolled Glide, and Parachute Descent models will return a possible impact point. Some parameters of these models are random variables of a probability distribution. Each time people use the model, they will get different impact points, so repeated use of these models will return many impact points, which obey the statistical distribution of the model itself. The number of repetitions is defined as the number of samples. Changing the number of samples will change the quality of the risk map, which means that the change in the risk value can be seen more clearly. A risk map with a smaller sample size can be generated quickly, but the quality will be reduced. The quality of the risk map with a larger sample size will be better, but it will take more time. If the sample size is large enough, the quality of the risk map will no longer be significantly improved, but the time spent will increase significantly, so it is crucial to choose the appropriate sample size.

- **Step width:** As mentioned in section 3.2.3, the flyaway model is different from the other three models. the probability value of hitting an area can be directly calculated through its probability density function. The step width controls the size of the area that is integrated each time through the probability density function. With smaller step sizes, better quality risk maps will be generated, because changes in risk values are better displayed, but please note that the cost of the integration operation is very high, so it is also essential to choose the appropriate step width.

- **Cell width:** The cell width is the width of each cell in the risk map. Each cell is defined as an impact point and has a risk value. A larger cell width means that more impacts may occur in this cell. If the cell width is too large, the risk value difference between two adjacent cells will be huge, so the displayed change in risk value is not very continuous. If the cell width is too small, then the risk value difference between cells is too small, So that it is easy to see no change in the value of risk.

The influence of these three parameters on generating the risk map is the focus of the upcoming evaluation.

4 Evaluation

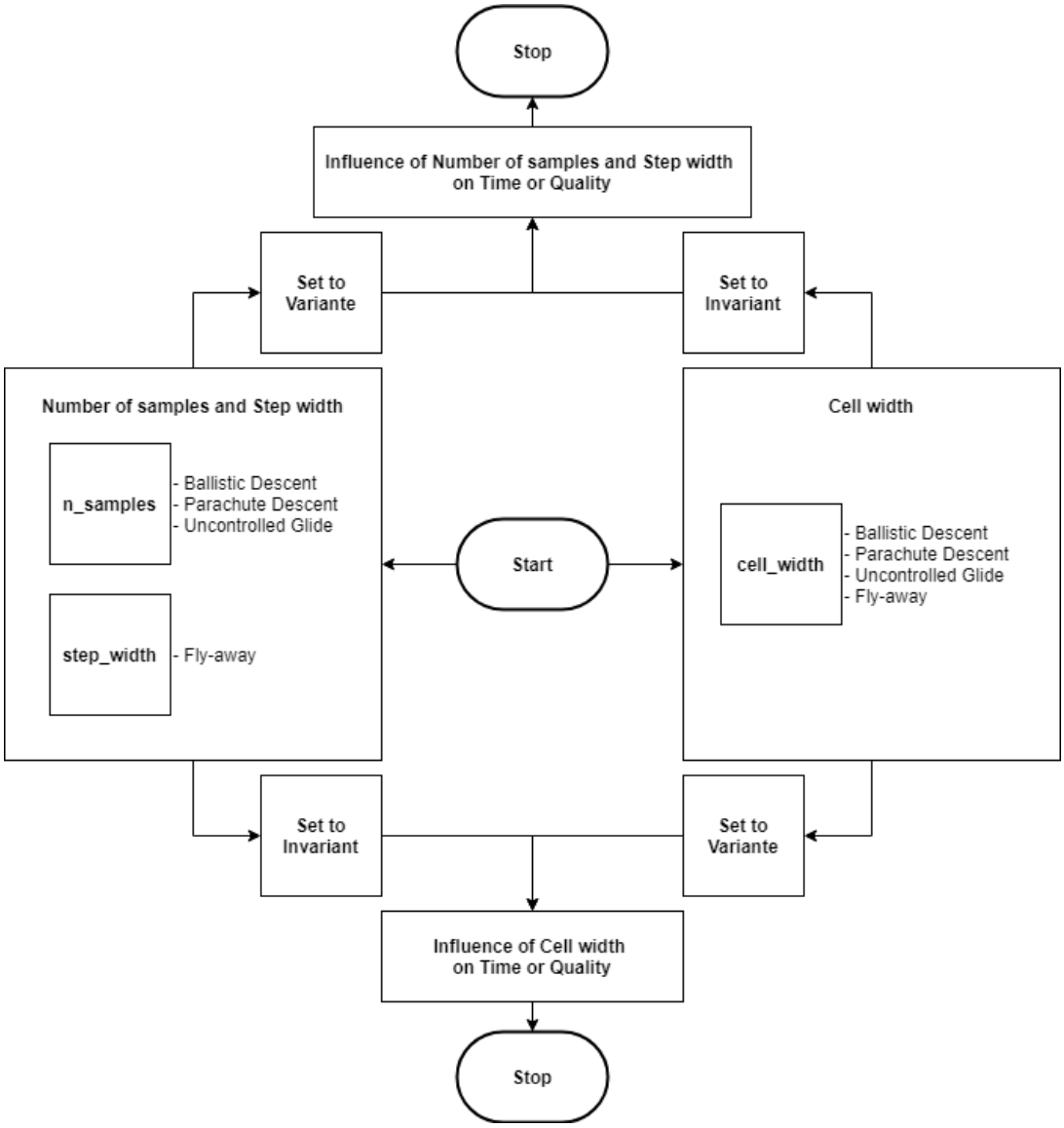

Figure 4.1: Evaluation process

Table 4.1: Information of test environment

Hardware or environment	Model or version
CPU	Inter(R) Core(TM) i5-7200U CPU @ 2.5GHz
RAM	8.00 GB
Graphics Card	Inter(R) HD Graphics 620
Development environment	Anaconda 4.7.12
Operation-system	Win 10 professional 64-bit

In this chapter, the time that the computer took to generate the risk map and the quality of the risk map will be evaluated in order to find out the optimal interval of parameters needed to generate a high-quality risk map in a short time. The whole evaluation process is based on the control variable method, and its flowchart 4.1 is given for easy understanding.

Finally, the risk value in the risk map is evaluated to ensure that this value is meaningful and reliable.

4.1 Time cost and quality

In section 3.2.8, it is mentioned that three parameters mainly determine the quality of the risk map. In this section, the influence of these three parameters on the risk map to generate a good quality risk map with low time cost for all four accident models will be evaluated, which are the number of samples, step width, and cell width. Because it takes different time for computers with different performance to generate the same risk map, the development environment used is also an essential factor affecting time, the hardware and development environment information of the computer used for testing are listed in Table 4.1.

4.1.1 Time cost

Time cost refers to the time it takes for the whole process that the computer uses the model to calculate the impact probability of each area, then use this probability to generate a risk map. The influence of parameters on it is as follows:

- **Number of samples and step width:** first, the cell width is set to a constant, `cell_width` $= 10$ in this case, change the size of the number of samples and step width, where `n_samples` $\in [10^4, 10^6]$ for the Ballstic Descent, Parachute Descent, Uncontrolled Glide and `step_width` $\in [2^0, 2^8]$ for the Fly-away. Each time `n_samples` or `step_width` is set to a different value, and then observe how the time of generating risk map changes. The results are shown in Figure 4.2. It is easy to find that the number of samples is directly proportional to the time cost, and the step width is inversely proportional to the time cost. In order to quickly

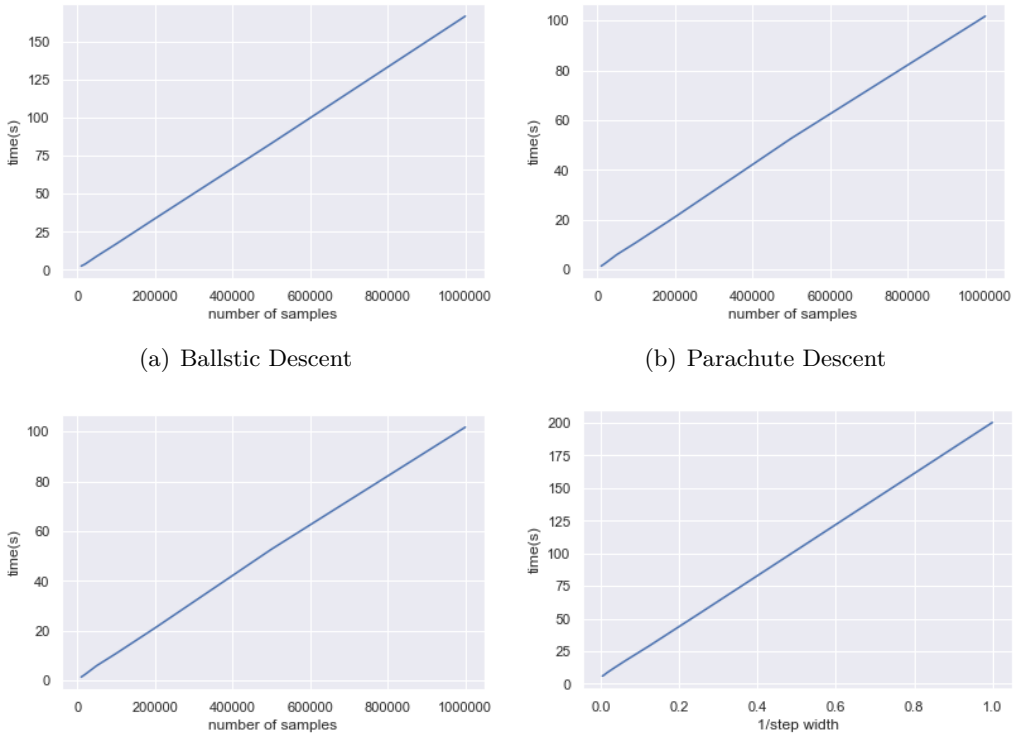

(a) Ballstic Descent

(b) Parachute Descent

(c) Uncontrolled Glide

(d) Fly-away

Figure 4.2: Influence of sample size and step width on time

generate the risk map, the time is controlled within ten seconds, because this time is only for the case where there is only one point on the flight path, for longer flight paths, time cost will multiply. `n_samples` $= 10^5$ and `step_width` $= 8$ should be the value that meets the requirements.

- **Cell width:** Next the number of samples and step width are set to constants, use the settings mentioned above: `n_samples` $= 10^5$ and `step_width` $= 8$, change the cell width: `cell_width` $\in [10^0, 10^3]$, and then observe how the calculation time changes. The results are shown in Figure 4.3.

  It can be found that for the ballistic descent, parachute descent, and uncontrolled glide model when the cell_width is changed, the value of the time cost change only slightly and can be ignored. Therefore, it can be considered that the change of cell_width does not affect the time cost. However, for the fly-away model, the time cost is inversely proportional to cell_width^2 (the area of the cell).

Finally, the evaluation results are summarized and listed in Table 4.2.

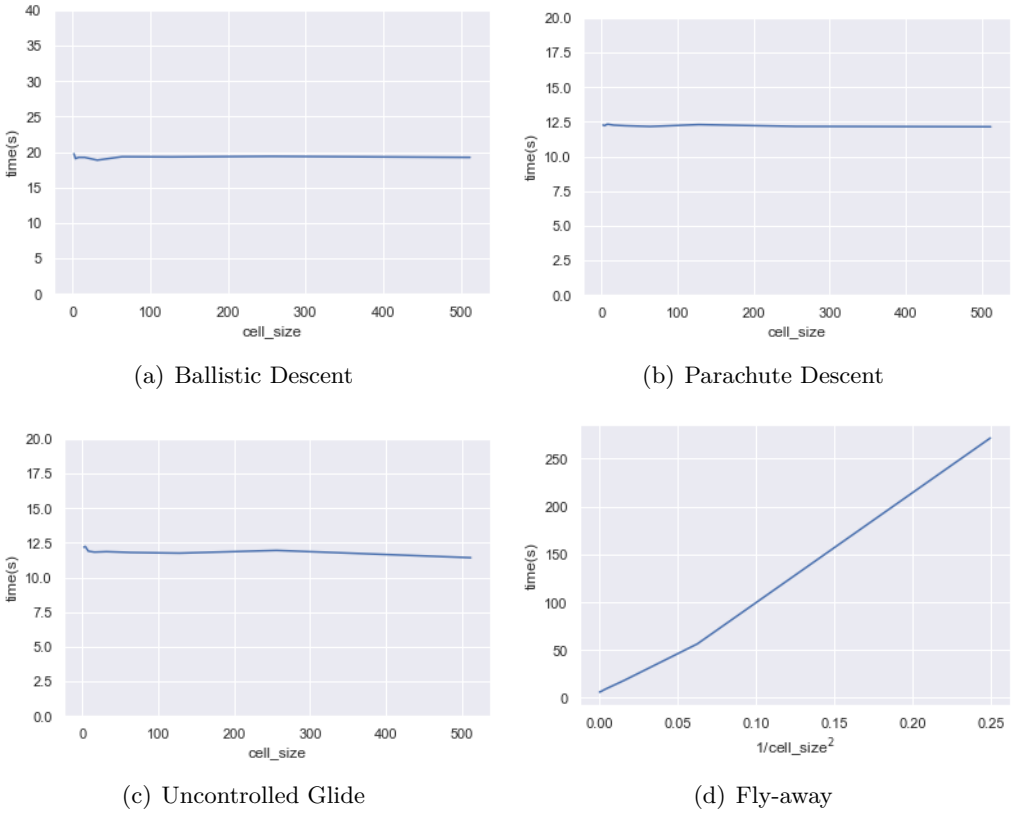

(a) Ballistic Descent

(b) Parachute Descent

(c) Uncontrolled Glide

(d) Fly-away

Figure 4.3: Influence of cell width on time

4.1.2 Quality

Quality refers to the quality of the generated risk map. The change in the risk value should be smooth, and the resolution should not be too low. The influence of several parameters on it is as follows:

- **Number of samples and step width:** Similarly, the cell width is set to a constant, `cell_width` $= 10$ in this case, change the size of the number of samples and step width, where `n_samples` $\in [10^4, 10^6]$ and `step_width` $\in [2^0, 2^8]$, now it is necessary to find the difference in quality of the risk map. Because there are too many images, only some examples are listed here. The risk maps of different accident models with different number of samples are shown in Figure 4.5, 4.6 and 4.7. Especially for the fly-away model, the risk maps with different step width are listed in Figure 4.8.

  By comparing these risk maps, the fact can be found that in some parameter intervals, the quality of the risk map will improve quickly, but after a specific value, there will no longer be significant changes. The results of the comparison are as follows: from the number of samples = 10000 to 100000 and step width

Table 4.2: Influence of parameters on time for different models

Time cost	**Number of samples**	**Step width**	**Cell width**
Ballistic Descent	Proportion	×	No influence
Parachute Descent	Proportion	×	No influence
Uncontrolled Glide	Proportion	×	No influence
Fly-away	×	Inverse proportion	Inverse proportion (Cell width^2)

= 128 to 32, the quality of the risk map has improved significantly, and then the speed of improvement will slow down afterward. Please also note that when the sample size is too large, points far from the center impact area may appear, such as in Figure 4.5(d), this is because some parameters are set through the normal distribution according to Table 3.1. If the sample size is too large, outliers that are far from the mean will appear. To sum up, a large `n_samples` is not recommended. On the one hand, if the `n_samples` is too large, it will cause unnecessary extra time. On the other hand, it is an effective way to avoid the occurrence of outliers.

Referring to the time cost in Figure 4.2, the time cost is controlled within 10s in this experiment. So set the `n_samples = 100000` , `step_width` = 32. With better hardware, the value can be increased for better quality, and the time cost remains at the same level.

- **Cell width:** Next the number of samples and step width are set to constant values according to the last part, with `n_samples` = 10^5 and `step_width` = 32, change the cell width: `cell_width` $\in [10^0, 10^3]$, then observe how the quality changes. The risk maps of different accident models with different cell width are shown in Figure 4.9, 4.10, 4.11 and 4.12.

  It can be found that for the Ballistic Descent, Parachute Descent, and Uncontrolled Glide models, their optimal cell widths (the cell width to generate the best quality of the risk map) are different because the size of their impact area is different for different models. The larger the impact area, the larger the optimal cell width. For Fly-away, the smaller the cell width, the better the quality of the risk map, but considering that the square of the cell width is inversely proportional to the time shown in Figure 4.3(d), too small cell width will cause colossal time cost, so the cell width should also be set within a reasonable range. According to the experiment, the range of optimal cell width is listed in Table 4.3.

4.1.3 Evaluation on the flight path

So far, the evaluation is based on one point on the flight path. A evaluation on several points on the flight path is also necessary. The optimal parameter settings according to Table 4.3 are used to generate a risk map, then observe the change of the risk map in figure 4.13, 4.14, 4.15, 4.16 and its time cost in figure 4.4.

Table 4.3: The range of optimal cell width

	Ballistic Descent	**Parachute Descent**
Cell width	4∼8	40∼80
Time cost with number of samples = 100000 and step width = 32	18.9s	11.7s
Time cost with number of samples = 500000 step width = 8	83.0s	52.6s
Time cost with number of samples = 1000000 step width = 2	166.8s	101.7s

	Uncontrolled Glide	**Fly-away**
Cell width	100∼200	8∼16
Time cost with number of samples = 100000 and step width = 32	11.8s	17.6s∼8.7s
Time cost with number of samples = 500000 step width = 8	50.4s	46.5s∼15.6s
Time cost with number of samples = 1000000 step width = 2	100.4s	164.6s∼45.8s

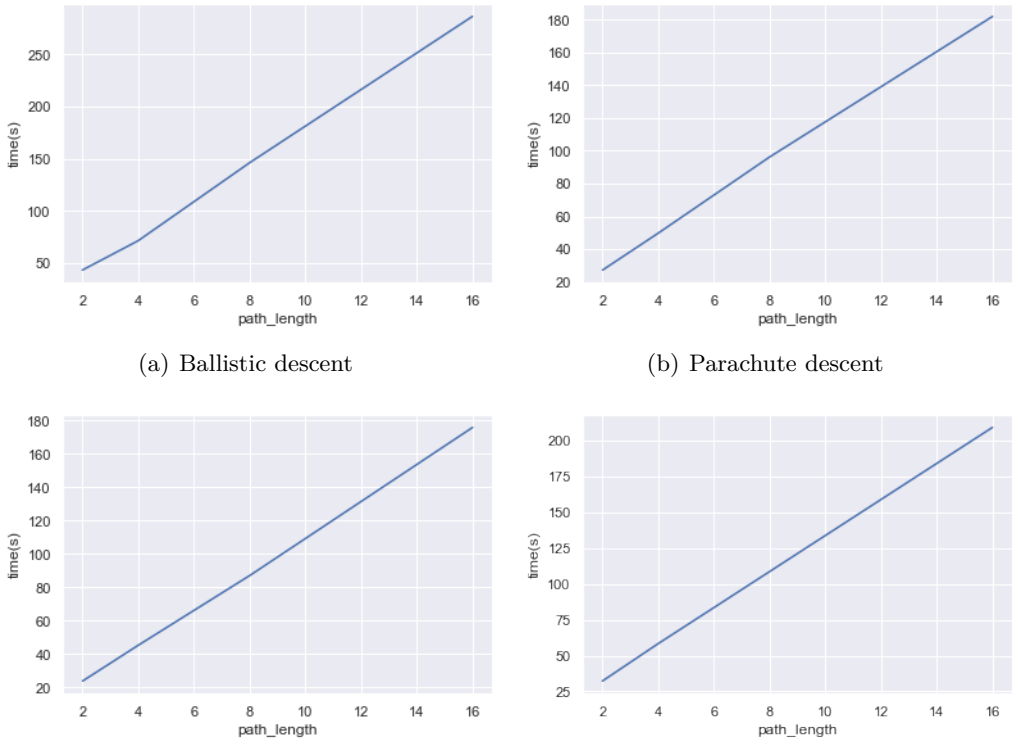

(a) Ballistic descent

(b) Parachute descent

(c) Uncontrolled descent

(d) Fly-away

Figure 4.4: Influence of path length on time

Finally, it can be found that the path length and the time required to generate the risk map are also proportional. With this information, a time-window can be derived to recalculate risk values for an altered trajectory-path and also determine a maximum time to calculate risk maps for unfinished trajectories.

4.2 Risk Value

In section 4.1, the parameters to create a high-quality risk map with low time cost are given. In this section, those parameters will be used to generate the risk map, and the risk value in the risk map will be evaluated. The goal of the evaluation is to make sure the risk value is within a reasonable range. This can prove that the calculation of the risk value is correct, and the risk value is meaningful and reliable.

According to section 2.9, due to differences between previous research, only approximate assessments can be made, the fatality rate from 10^{-9} to 10^{-6} is selected as the criterion. Because this fatality rate is the probability for the fatality of anyone, and it is also the range of casualty expectations.

Next, the casualty expectation given by the casualty model of this thesis will be

Table 4.4: Average of risk values from different models

Accident type	**Average of risk values**
Ballistic Descent	$1.14 \cdot 10^{-8}$
Uncontrolled Glide	$7.19 \cdot 10^{-8}$
Parachute Descent	$7.75 \cdot 10^{-9}$
Fly-away	$2.01 \cdot 10^{-8}$

compared with the reasonable range of risk value mentioned in the previous paragraph. Please note that in the evaluation of section 4.1, the calculated probability of impact is the probability that under the condition that the accident has already happened. This value should be multiplied by the probability of accidents. The result of this multiplication is the probability of impacting the ground when the aircraft is flying normally and has not broken down yet-then multiplied by the output value of the casualty estimation model to get the required casualty estimate. In order to simplify the test and for the sake of conservativeness, the maximal value 10^{-6} from table 2.1 is used as the probability of accidents, the population density required for the casualty estimation model is set to the average population density of Germany: $\rho = 432$, and the shielding factor is set to the intermediate value of the sheltered and uncovered objects: $p_s = 0.5$. Then all the risk values in the risk map are summed up and divided by the number of grids with non-zero values in the risk map. This gives the average of risk values. The final results are listed in Table 4.4.

The average of risk values of the four models are all in the range of 10^-9 to 10^-6, so the calculation of the risk value is correct, and the risk value is meaningful and reliable.

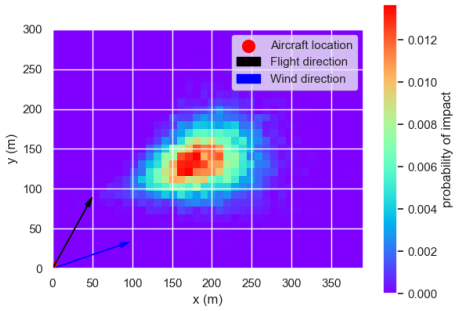

(a) Number of samples = 10000

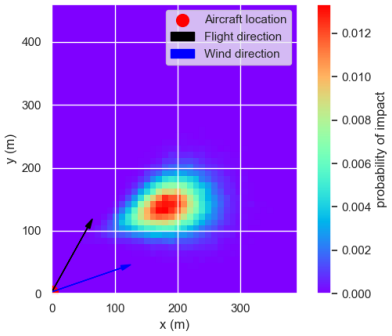

(b) Number of samples = 100000

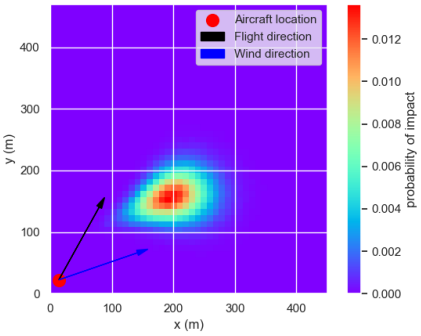

(c) Number of samples = 500000

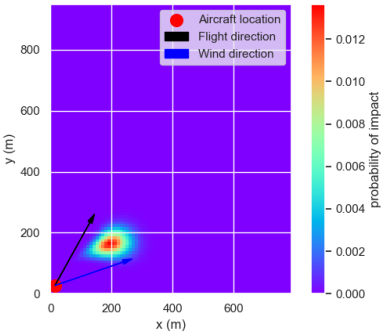

(d) Number of samples = 1000000

Figure 4.5: Ballistic descent with cell width = 10

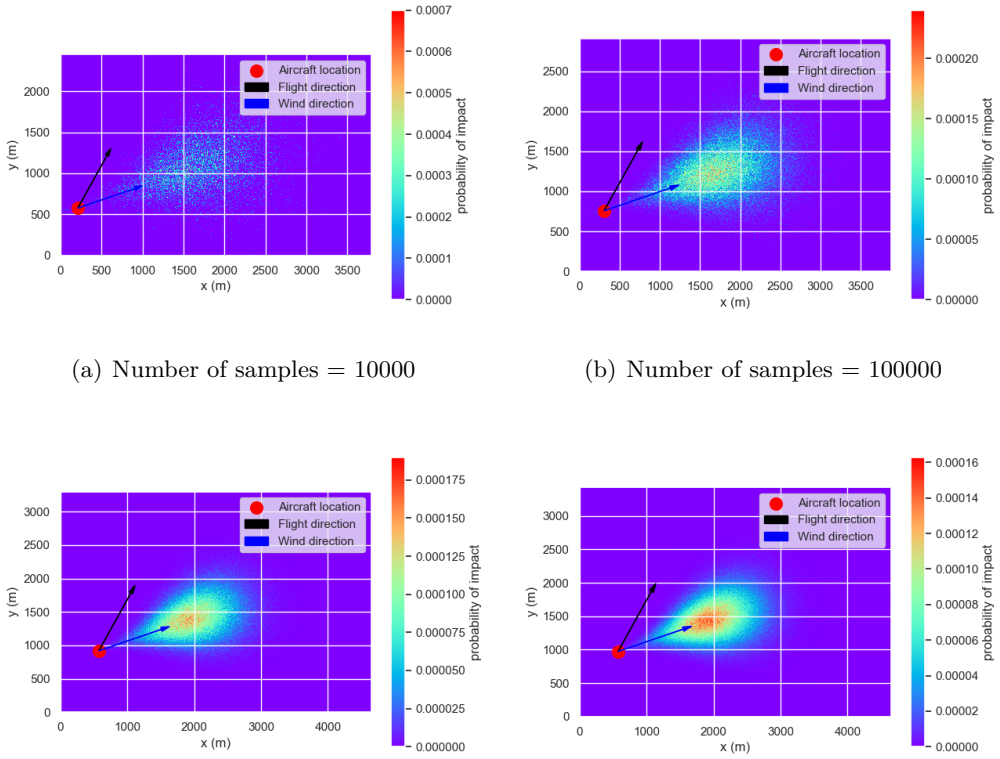

(a) Number of samples = 10000

(b) Number of samples = 100000

(c) Number of samples = 500000

(d) Number of samples = 1000000

Figure 4.6: Parachute descent with cell width = 10

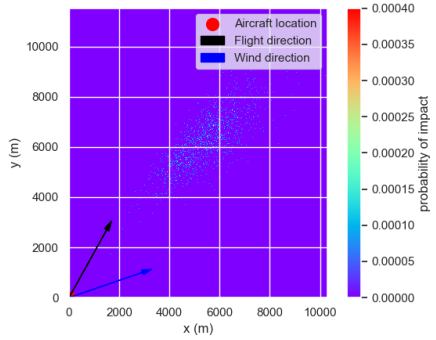

(a) Number of samples = 10000

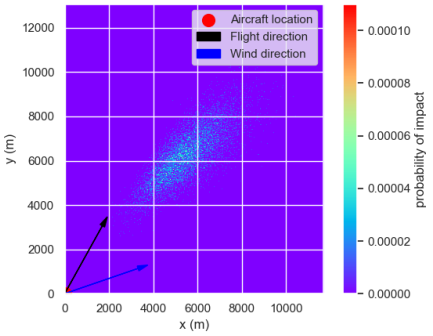

(b) Number of samples = 100000

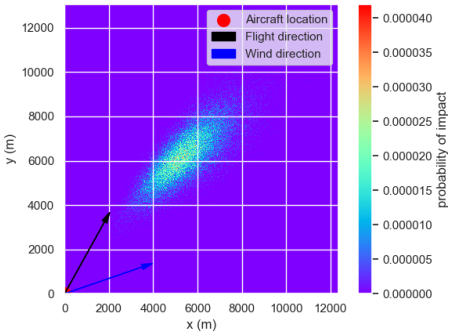

(c) Number of samples = 500000

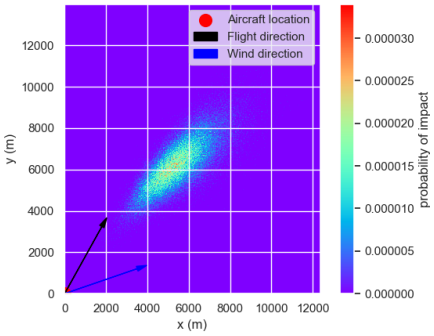

(d) Number of samples = 1000000

Figure 4.7: Uncontrolled glide with cell width = 10

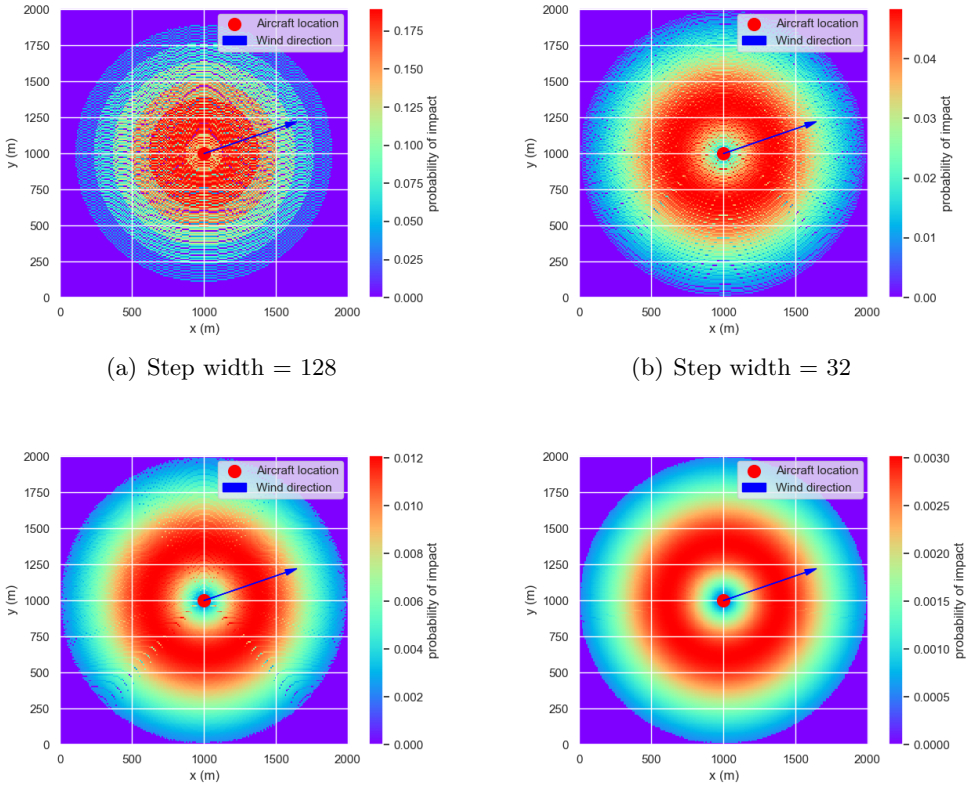

(a) Step width = 128

(b) Step width = 32

(c) Step width = 8

(d) Step width = 2

Figure 4.8: Fly-away with cell width = 10

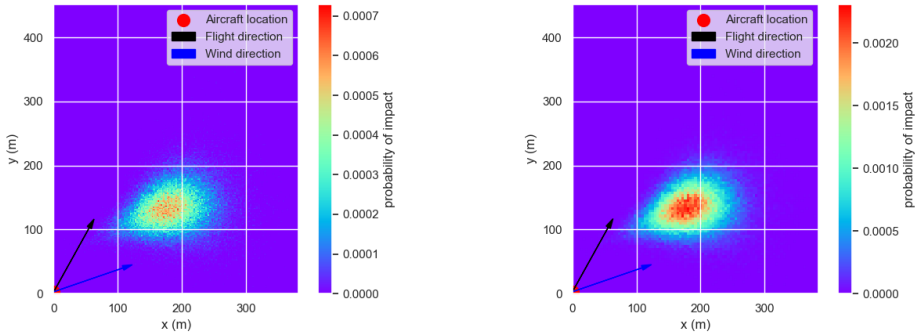

(a) Cell width = 2

(b) Cell width = 4

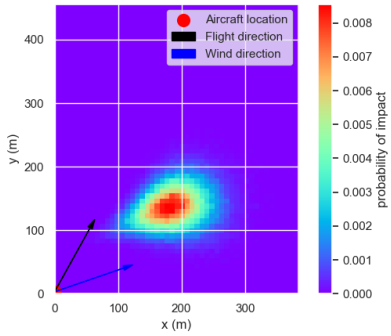

(c) Cell width = 8

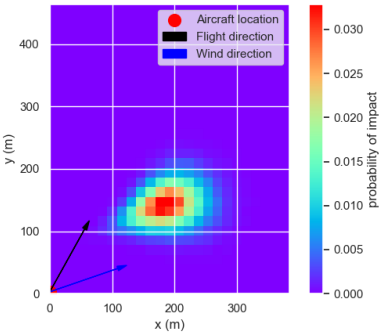

(d) Cell width = 16

Figure 4.9: Ballistic descent with number of samples = 100000

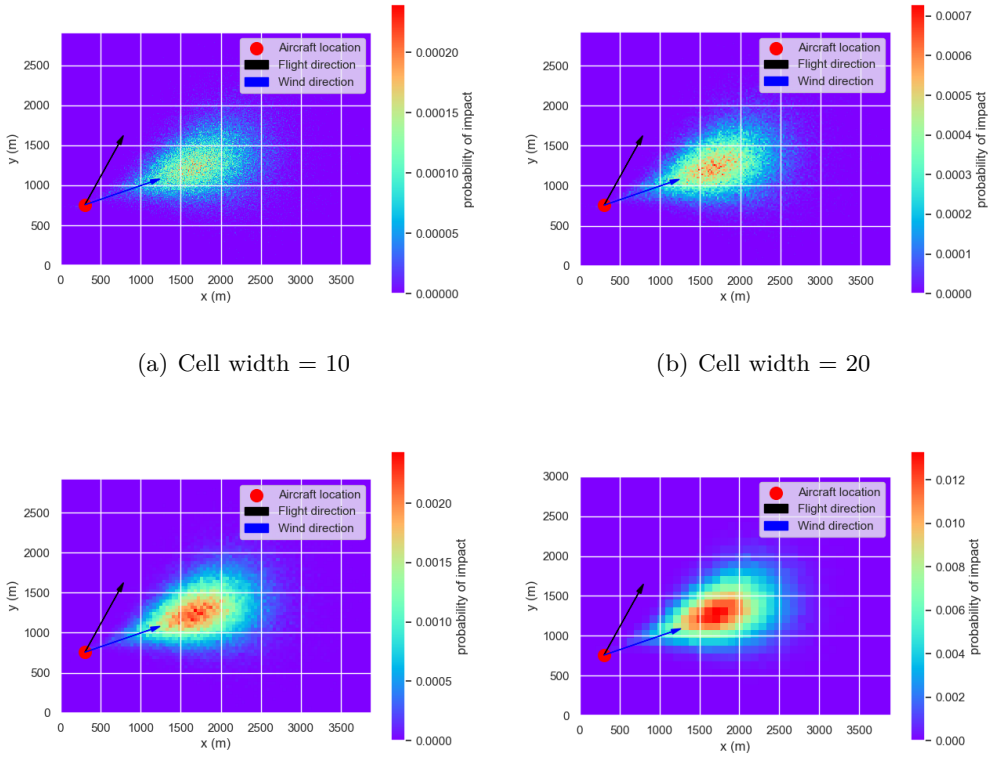

(a) Cell width = 10

(b) Cell width = 20

(c) Cell width = 40

(d) Cell width = 80

Figure 4.10: Parachute descent with number of samples = 100000

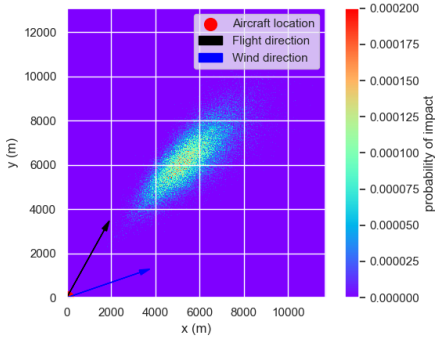

(a) Cell width = 25

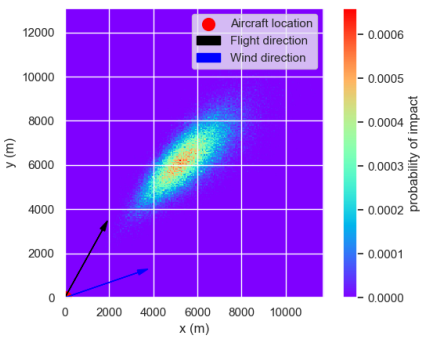

(b) Cell width = 50

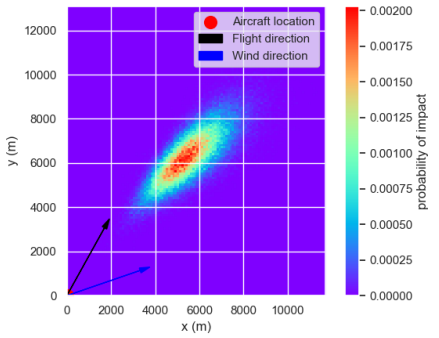

(c) Cell width = 100

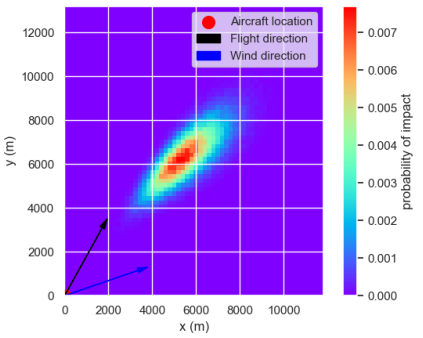

(d) Cell width = 200

Figure 4.11: Uncontrolled glide with number of samples = 100000

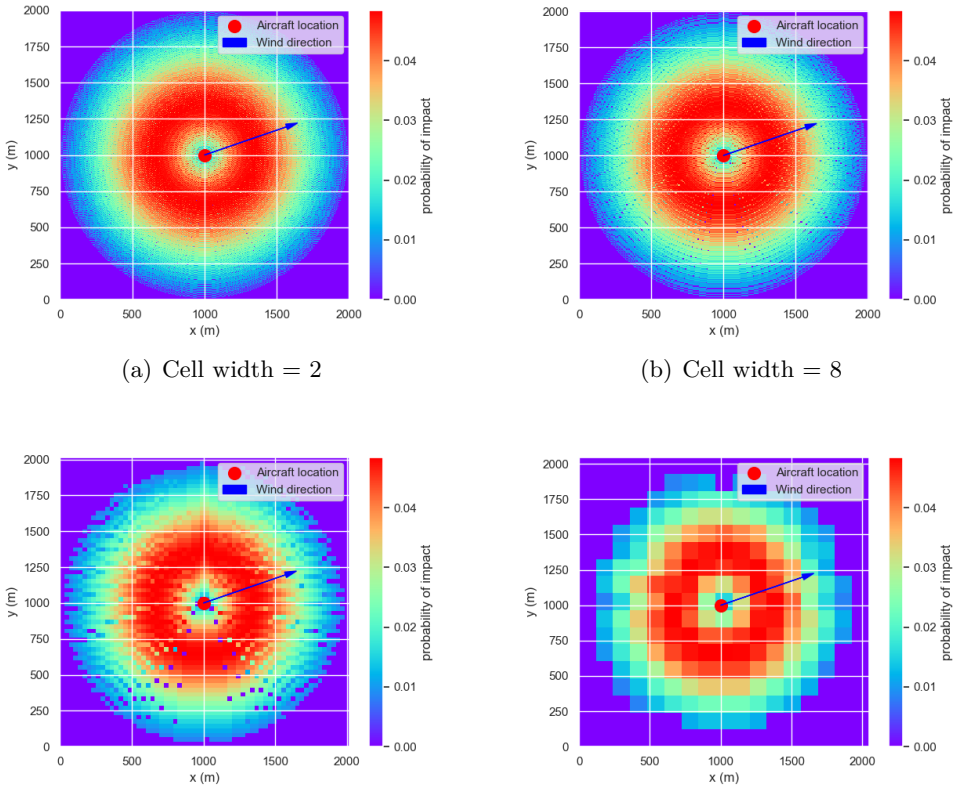

(a) Cell width = 2

(b) Cell width = 8

(c) Cell width = 32

(d) Cell width = 128

Figure 4.12: Fly-away with step width = 32

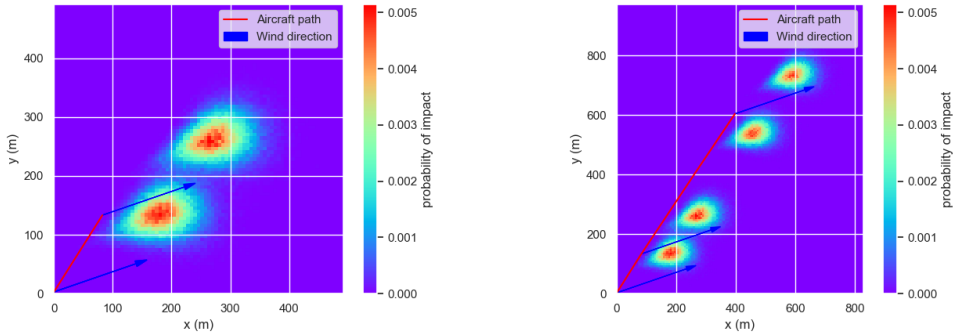

(a) Path length = 2

(b) Path length = 4

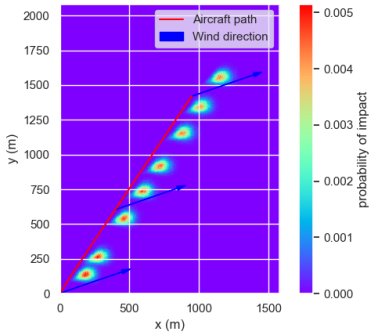

(c) Path length = 8

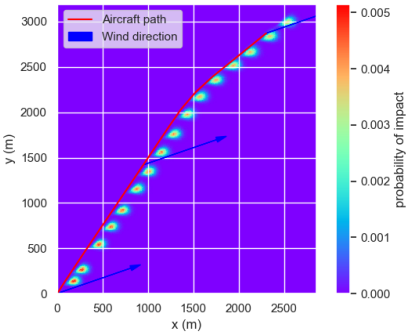

(d) Path length = 16

Figure 4.13: Ballistic descent with cell width = 6, number of samples = 100000

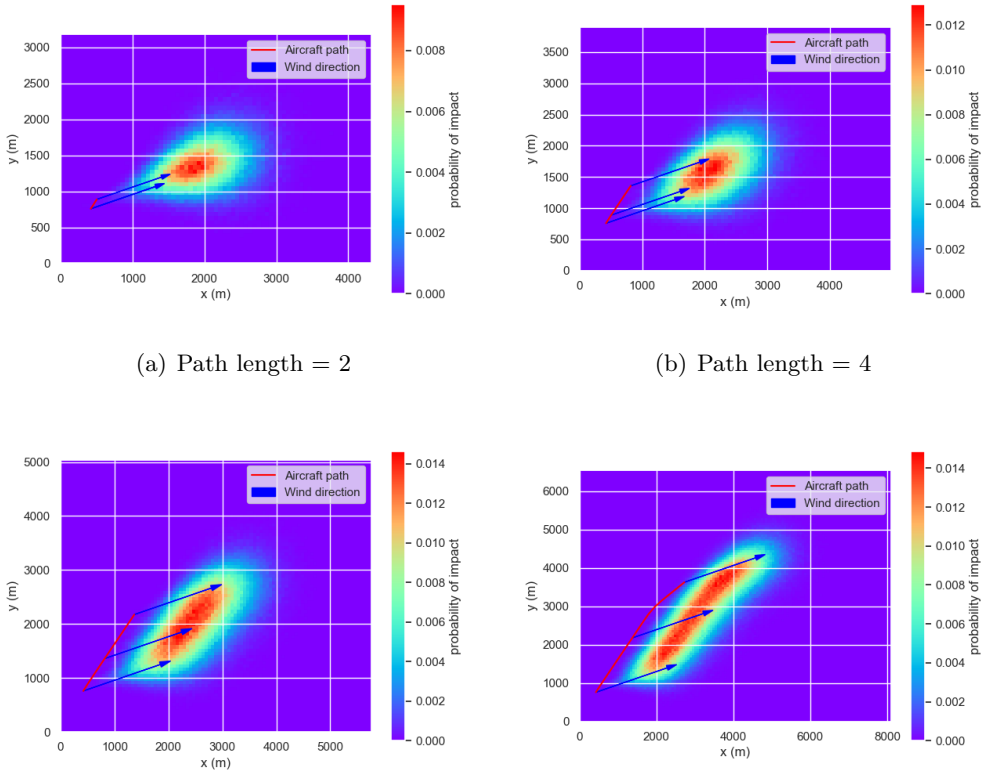

(a) Path length = 2

(b) Path length = 4

(c) Path length = 8

(d) Path length = 16

Figure 4.14: Parachute descent with cell width = 60, number of samples = 100000

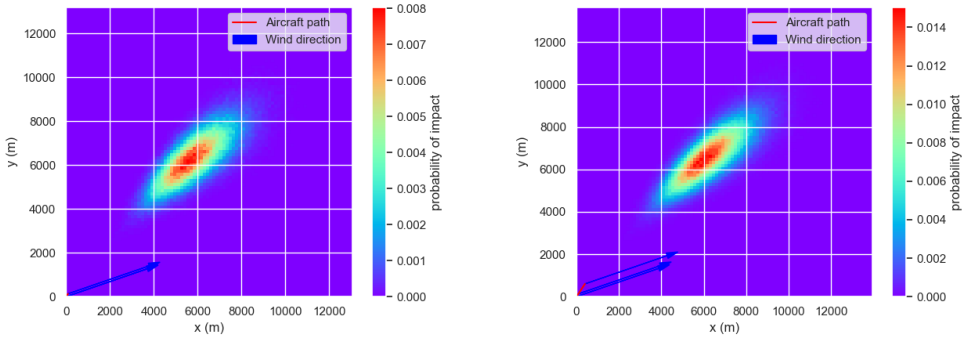

(a) Path length = 2

(b) Path length = 4

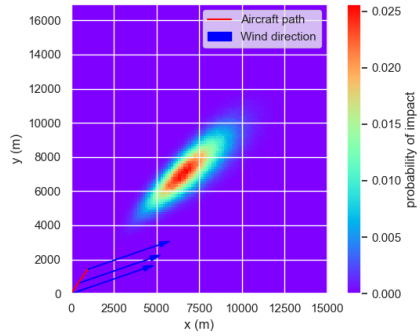

(c) Path length = 8

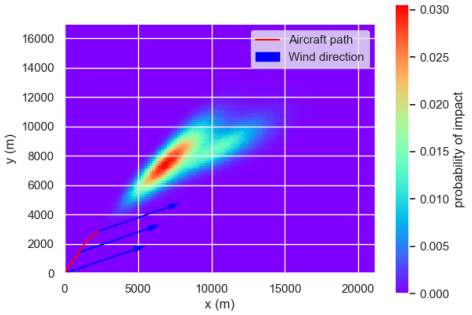

(d) Path length = 16

Figure 4.15: Uncontrolled glide with cell width = 150, number of samples = 100000

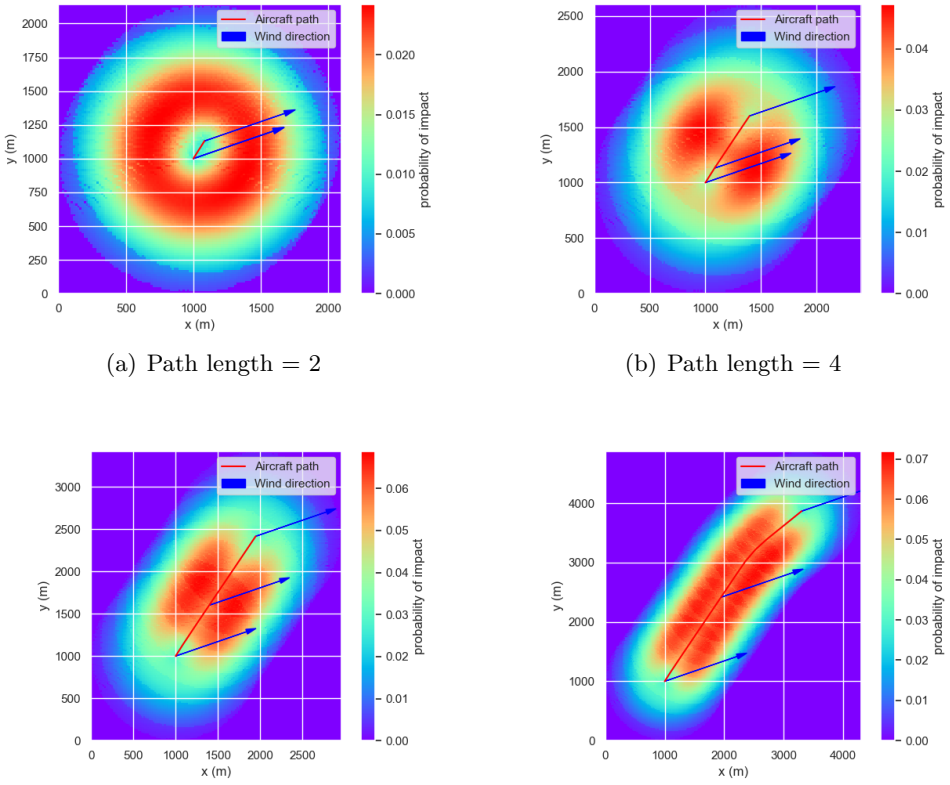

(a) Path length = 2

(b) Path length = 4

(c) Path length = 8

(d) Path length = 16

Figure 4.16: Fly-away with cell width = 16, step width = 8

5 Future Work

5.1 Advanced Method to calculate Probability of Accidents

In section 2.4, the data in Table 2.1 was directly used as the probability of accidents. However, there are more advanced and more accurate methods, such as the method mentioned in [1], the UAV's real-time data such as GPS Count, GPS Status, Remaining Battery, Battery Voltage, and Telemetry Health, can be obtained by the computer and sensors on the UAV. Bringing these real-time data into the Bayesian Belief Network can make a more accurate prediction of the probability of a UAV failure.

5.2 Calculation Method of Accident Models

In principle, the calculation of the impact probability for each grid in the risk map should be completed by double integration based on the probability density function, but because the time of calculation spent on the test computer is too long, a smarter method is used in this thesis to reduce the time cost. For example, impact points are obtained by sampling, and afterward converting to impact probability instead of integration; the ring area centered on the location of the aircraft is integrated instead of all grids. The cost of this method is to reduce the accuracy of the prediction. So it is necessary to find a method that can reduce the time cost but does not reduce the quality of the risk map, such as using integration more efficiently.

5.3 Large Scale Experiment

The parameter settings for the case study are given in Table 3.1. Obviously, this is the parameter of just one type of UAV. There are many types of UAVs in reality. Their parameters are different, so using more types of UAVs to conduct experiments makes the experiments more complex but also more complete. In section 3.2.5 and section 3.2.6, the population density map, and the shelter map are only obtained through simulation, or the average value is directly used. In the future, real urban areas can be used for a more meaningful experiment, the data for shelters could be gathered through VGI-Projects like OSM, and the population density map could be exchanged with data sets of mobile phone data usage, which would create real-world instances with a higher dynamic.

6 Conclusions

The main goal of this thesis is to generate a UAV's risk map in flight and in a fast dynamically manner to find out the time that computer took to generate the risk map and how to optimize the time cost and also the quality of the risk map. In other words: Generating a risk map of sufficient quality in a short time to avoid high-risk areas.

Four accident models were used to predict the possible impact points of accidents. The wind model was implemented to bring the effect of wind in the location of impact points. Then the casualty estimation model, in combination with population density, the type of shelter, and related UAV parameters, was used to estimate the number of casualties.

The risk map was generated based on the output of models, and three parameters had a significant influence on the generation of the risk map. The control variable method is used for parameter evaluation. By evaluating those parameters, the optimal ranges of those parameters were found to generate the risk map with sufficient quality quickly. Before the evaluation, the parameter settings of all models were based on Table 3.1.

According to table 4.2 and section 4.1.2, for Ballistic Descent, Parachute Descent, and Uncontrolled Glide models, the number of samples is directly proportional to the time to generate the risk map, which means that increasing the number of samples will inevitably increase the time cost. However, in order to increase the quality of the risk map, it is also necessary to increase the number of samples. The step width for the Fly-away model is precisely the opposite. It needs to be lowered to obtain higher quality while bearing higher time costs. According to the optimal parameter intervals given in Table 4.3, when number of samples = 10000, step width = 32, a good balance can be reached between quality and cost.

It can also be found in Table 4.2 that for Ballistic Descent, Parachute Descent, and Uncontrolled Glide models, the change in cell width has no effect on the time cost, so the best value can be chosen regardless of cost. According to Table 4.3, select the median value of the best interval, cell width for Ballistic Descent = 6, for Parachute Descent = 60, for Uncontrolled Glide = 150, and note that their optimal cell widths are varying for different models. This is because their possible crash areas are different in size, which requires special attention when generating risk maps in the future. For Fly-away, the square of the cell width is inversely proportional to the time cost, so its value should be carefully selected to prevent the time cost from being too large. An optimal value given in Table 4.2 is 12.

Evaluation on the flight path in section 4.1.3 shows that the time required to generate a risk map is directly proportional to the length of the flight path if other parameters are determined. This is helpful for estimating the time required to generate a risk map for a longer flight path, which also means that the additional time spent by a longer

flight path is controllable.

With the rapid popularization of UAV technology, it is becoming more and more necessary to improve the risk management and risk control of UAVs, for which trajectory optimization is a very effective method. A risk map with sufficient accuracy, and that can be generated at an acceptable time is essential for this method and deserve further exploration.

Acknowledgment

The author would like to thank the Department of Informatics headed by Prof. Dr. Sven Hartmann for their strong support to students, providing students with an excellent learning environment, sufficient learning resources, and high-quality thesis topics.

Thanks to Dr. Umut Durak for his previous work in the related field. Thanks to Gerrit Burmester, M.Sc, for his full support and his help in research direction and thesis writing.

Thanks to Run Lü, M.Sc for his help in aerophysics, Dongai Liu, M.Sc for his help in python scientific computing, and finally to the family for their support for studying abroad.

Bibliography

[1] Ancel, Ersin ; Capristan, Francisco M. ; Foster, John V. ; Condotta, Ryan C.: Real-time risk assessment framework for unmanned aircraft system (uas) traffic management (utm). In: *17th AIAA Aviation Technology, Integration, and Operations Conference*, 2017, S. 3273

[2] Betts, John T.: Survey of numerical methods for trajectory optimization. In: *Journal of guidance, control, and dynamics* 21 (1998), Nr. 2, S. 193–207

[3] Clothier, Reece A. ; Walker, Rodney A.: Determination and evaluation of UAV safety objectives. (2006)

[4] Clothier, Reece A. ; Walker, Rodney A.: The safety risk management of unmanned aircraft systems. In: *Handbook of unmanned aerial vehicles* (2015), S. 2229–2275

[5] Clothier, Reece A. ; Walker, Rodney A. ; Fulton, Neale ; Campbell, Duncan A.: A casualty risk analysis for unmanned aerial system (UAS) operations over inhabited areas. (2007)

[6] Clothier, Reece A. ; Williams, Brendan P. ; Fulton, Neale L.: Structuring the safety case for unmanned aircraft system operations in non-segregated airspace. In: *Safety science* 79 (2015), S. 213–228

[7] Clothier, Reece A. ; Wu, Paul P.: A review of system safety failure probability objectives for unmanned aircraft systems. In: *Proceedings of the 11th International Probabilistic Safety Assessment and Management (PSAM11) Conference and the Annual European Safety and Reliability (ESREL 2012) Conference.*, 2012

[8] Council, Range C.: Range safety criteria for unmanned air vehicles. In: *Series Range Safety Criteria for Unmanned Air Vehicles. White Sands Missile Range, NM: Range Safety Group of the Range Commander's Council at the White Sands Missile Range* (1999)

[9] Council, Range C.: Standard 321-07 "common risk criteria standards for national test ranges: Supplement". In: *USA Dept. of Defense* (2007)

[10] Cour-Harbo, Anders la: Quantifying risk of ground impact fatalities for small unmanned aircraft. In: *Journal of Intelligent & Robotic Systems* 93 (2019), Nr. 1-2, S. 367–384

[11] Dalamagkidis, Konstantinos ; Valavanis, Kimon P. ; Piegl, Les A.: Evaluating the risk of unmanned aircraft ground impacts. In: *2008 16th mediterranean conference on control and automation* IEEE, 2008, S. 709–716

[12] Denney, Ewen ; Pai, Ganesh: Safety considerations for UAS ground-based detect and avoid. In: *2016 IEEE/AIAA 35th Digital Avionics Systems Conference (DASC)* IEEE, 2016, S. 1–10

[13] Freeman, Paul ; Balas, Gary J.: Actuation failure modes and effects analysis for a small UAV. In: *2014 American control conference* IEEE, 2014, S. 1292–1297

[14] Freeman, Paul M.: Reliability assessment for low-cost unmanned aerial vehicles. (2014)

[15] JAA, Eurocontro: *Eurocontrol UAV Task-Force Final Report. A Concept For European Regulations For Civil Unmanned Aerial Vehicles (UAVs).* 2004

[16] Kang, Chaogui ; Liu, Yu ; Ma, Xiujun ; Wu, Lun: Towards estimating urban population distributions from mobile call data. In: *Journal of Urban Technology* 19 (2012), Nr. 4, S. 3–21

[17] King, David W. ; Bertapelle, Allen ; Moses, Chad: UAV failure rate criteria for equivalent level of safety. In: *International helicopter safety symposium* Bd. 8, 2005

[18] La Cour-Harbo, Anders ; Schioler, H: Ground impact probability distribution for small unmanned aircraft in ballistic descent. In: *Reliability engineering and system safety Submitted* (2017)

[19] Lin, Xunguo ; Fulton, Neale L. ; Horn, Mark E.: Quantification of high level safety criteria for civil unmanned aircraft systems. In: *2014 IEEE Aerospace Conference* IEEE, 2014, S. 1–13

[20] Lum, Christopher ; Waggoner, Blake: A risk based paradigm and model for unmanned aerial systems in the national airspace. In: *Infotech@ Aerospace 2011.* 2011, S. 1424

[21] Oster Jr, Clinton V. ; Strong, John S. ; Zorn, C K.: Analyzing aviation safety: Problems, challenges, opportunities. In: *Research in transportation economics* 43 (2013), Nr. 1, S. 148–164

[22] Ponda, Sameera ; Kolacinski, Richard ; Frazzoli, Emilio: Trajectory optimization for target localization using small unmanned aerial vehicles. In: *AIAA guidance, navigation, and control conference*, 2009, S. 6015

[23] Primatesta, Stefano ; Cuomo, Luca S. ; Guglieri, Giorgio ; Rizzo, Alessandro: An innovative algorithm to estimate risk optimum path for unmanned aerial vehicles in urban environments. In: *Transportation research procedia* 35 (2018), S. 44–53

[24] Primatesta, Stefano ; Rizzo, Alessandro ; Cour-Harbo, Anders la: Ground risk map for Unmanned Aircraft in Urban Environments. In: *Journal of Intelligent & Robotic Systems* (2018), S. 1–21

[25] Rubio-Hervas, Jaime ; Gupta, Abhishek ; Ong, Yew-Soon: Data-driven risk assessment and multicriteria optimization of UAV operations. In: *Aerospace Science and Technology* 77 (2018), S. 510–523

[26] Sussmann, Hector J. ; Willems, Jan C.: 300 years of optimal control: from the brachystochrone to the maximum principle. In: *IEEE Control Systems Magazine* 17 (1997), Nr. 3, S. 32–44

[27] Venkataraman, Raghu ; Lukátsi, Márk ; Vanek, Bálint ; Seiler, Peter: Reliability assessment of actuator architectures for unmanned aircraft. In: *IFAC-PapersOnLine* 48 (2015), Nr. 21, S. 398–403

[28] Waggoner, Blake: *Developing a risk assessment tool for unmanned aircraft system operations*, University of Washington, Diss., 2010

[29] Weibel, Roland ; Hansman, R J.: Safety considerations for operation of different classes of UAVs in the NAS. In: *AIAA 4th Aviation Technology, Integration and Operations (ATIO) Forum*, 2004, S. 6244

[30] Wu, Paul P. ; Clothier, Reece A.: The development of ground impact models for the analysis of the risks associated with unmanned aircraft operations over inhabited areas. In: *Proceedings of the 11th probabilistic safety assessment and management conference (PSAM11) and the annual European safety and reliability conference (ESREL 2012)*, 2012